Earth and Planetary Science Letters 351–352 (2012) 54–69

Contents lists available at SciVerse ScienceDirect

Earth and Planetary Science Letters

journal homepage: www.elsevier.com/locate/epsl

Dynamics of the Laschamp geomagnetic excursion from Black Sea sediments

N.R. Nowaczyk [a,*], H.W. Arz [a,b], U. Frank [a], J. Kind [a,c], B. Plessen [a]

[a] Helmholtz Centre Potsdam, GFZ German Research Centre for Geosciences, Section 5.2 – Climate Dynamics and Landscape evolution, 14473 Potsdam, Germany
[b] Leibnitz Institute for Baltic Sea Research Warnemünde, 18119 Rostock, Germany
[c] ETH Zürich, Institute of Geophysics, 8092 Zürich, Switzerland

ARTICLE INFO

Article history:
Received 24 February 2012
Received in revised form
25 June 2012
Accepted 26 June 2012
Editor: J. Lynch-Stieglitz
Available online 29 August 2012

Keywords:
Black Sea
paleomagnetism
Laschamp excursion
Mono Lake excursion
relative paleointensity
virtual geomagnetic poles (VGP)

ABSTRACT

Investigated sediment cores from the southeastern Black Sea provide a high-resolution record from mid latitudes of the Laschamp geomagnetic polarity excursion. Age constraints are provided by 16 AMS ^{14}C ages, identification of the Campanian Ignimbrite tephra (39.28 ± 0.11 ka), and by detailed tuning of sedimentologic parameters of the Black Sea sediments to the oxygen isotope record from the Greenland NGRIP ice core. According to the derived age model, virtual geomagnetic pole (VGP) positions during the Laschamp excursion persisted in Antarctica for an estimated 440 yr, making the Laschamp excursion a short-lived event with fully reversed polarity directions. The reversed phase, centred at 41.0 ka, is associated with a significant field intensity recovery to 20% of the preceding strong field maximum at ~50 ka. Recorded field reversals of the Laschamp excursion, lasting only an estimated ~250 yr, are characterized by low relative paleointensities (5% relative to 50 ka). The central, fully reversed phase of the Laschamp excursion is bracketed by VGP excursions to the Sargasso Sea (~41.9 ka) and to the Labrador Sea (~39.6 ka). Paleomagnetic results from the Black Sea are in excellent agreement with VGP data from the French type locality which facilitates the chronological ordering of the non-superposed lavas that crop out at Laschamp–Olby. In addition, VGPs between 34 and 35 ka reach low northerly to equatorial latitudes during a clockwise loop, inferred to be the Mono lake excursion.

1. Introduction

Geomagnetic field excursions are short episodes ($< 10^4$ yr) when virtual geomagnetic poles (VGPs) move away from the area of normal secular variation at high latitudes (Laj and Channell, 2007). The first excursion reported to have occurred during the geomagnetic normal polarity Brunhes Chron, and recorded in volcanic rocks, is the Laschamp excursion (Bonhommet and Babkine, 1967; Gillot et al., 1979; Guillou et al., 2004; Plenier et al., 2007). At its type locality in the French Massif Central, several laterally distributed, non-superposed lava flows (at Laschamp, Olby, Louchadière and Royat) carry different intermediate and nearly fully reversed polarity magnetisation directions. Although results were doubted because of self-reversal in some parts of the lavas (e.g., Heller and Petersen, 1982; Krása et al., 2005), a summary of various modern studies on these flows yielded consistent and reliable paleomagnetic data (Plenier et al., 2007). The lava flows from the Massif Central are also characterized by low paleointensities (Chauvin et al., 1989; Roperch et al., 1988). The most recent dating (Singer et al., 2009) yielded radiometric (^{40}Ar/^{39}Ar, K–Ar, ^{230}Th–^{238}U) ages of the different lava flows that are statistically indistinguishable, with a mean age of 40.70 ± 0.95 ka b2k. The compilation of Singer et al. (2009) includes older datings at Laschamp (Guillou et al., 2004) and an age determined for a contemporary lava flow from New Zealand (Cassata et al., 2008) with a non-dipolar direction and a low paleointensity of 2.5 μT (Mochizuki et al., 2006). Other volcanic records of the Laschamp excursion come from Hawaii (e.g., Laj et al., 2011). New datings of the Icelandic Skálamælifell lavas, initially also related to the Laschamp excursion (Levi et al., 1990), with VGPs close to the Laschamp/Olby VGPs, now give an age of 95 ka, thus indicating that these lavas must have recorded a different excursion (Jicha et al., 2011).

In principle, at a first sight, volcanic rocks appear to be ideal paleomagnetic recorders, providing the full geomagnetic field vector with inclination, declination, and absolute paleointensity. Moreover, they can be numerically dated by radiometric techniques (e.g., K/Ar, ^{40}Ar/^{39}Ar). However, the remanence of volcanics are only spot readings of geomagnetic field variations, and, because of limitations in the precision of the dating methods, ages of volcanic rocks that erupted closely in time cannot be resolved, as is the case for the French lavas that recorded the Laschamp excursion (Singer et al., 2009). In contrast, sediments can continuously record geomagnetic field variations, with the limitation of providing only relative intensity variations. However, many types of sediments did not record any directional excursion as a result of post-depositional lock-in and smoothing of the remanence directions (Roberts and Winklhofer, 2004). This leaves a fragmentary record and raises many unanswered questions about the true nature of geomagnetic excursions (Roberts, 2008). Some sedimentary environments are

* Corresponding author.
E-mail address: norbert.nowaczyk@gfz-potsdam.de (N.R. Nowaczyk).

0012-821X/$ - see front matter © 2012 Elsevier B.V. All rights reserved.
http://dx.doi.org/10.1016/j.epsl.2012.06.050

able to record geomagnetic excursions. The Laschamp excursion is within the reach of radiocarbon dating and most coring techniques, so it is relatively well studied. Northern high latitude sites yielded the first sedimentary evidence for geomagnetic excursions, with simple age models based on calcareous nannofossil biostratigraphy (e.g., Bleil and Gard, 1989; Nowaczyk and Baumann, 1992). Later, high-resolution records with high precision dating became available (e.g., Channell, 2006; Channell et al., 2012; Laj et al., 2000; Lund et al., 2005; Lund et al., 2006; Nowaczyk et al., 2003). Depending on the sedimentary composition, absolute and/or relative ages of different precision can be determined by various methods, such as correlation of stratigraphic data to dated reference records (e.g., oxygen isotope data or pollen), by tephrochronology, or by radiometric dating techniques (e.g., ^{14}C and U/Th). We report here a well dated record from the Black Sea Basin. Our study focuses on limnic Black Sea sediments and we present high resolution paleomagnetic and environmental records covering most of the last glacial period.

2. Geological setting

The Black Sea is currently the Earth's largest anoxic marine basin. Laminated Holocene, but also Eemian and older interglacial sediments, document a strong link between interglacial sea level high stands and the development of anoxia in the basin (Ross and Degens, 1974). During the last glacial period, however, the basin was disconnected from the Mediterranean Sea as a result of a glacioeustatically controlled decrease in global sea level below the sill of the Bosphorus (modern minimum water depth 36 m). During this period, the basin was filled with a well oxygenated freshwater body where oxic sediments were deposited (Badertscher et al., 2011; Ross and Degens, 1974; Winguth et al., 2000). The uppermost Black Sea deposits document a basin-wide succession of glacial to early Holocene lacustrine clayey muds (Unit III), a finely laminated Holocene marine sapropel (Unit II), and coccolith oozes (Unit I). More detailed descriptions are given by Major et al. (2006) and Kwiecien et al. (2008). The underlying glacial limnic sediments generally consist of fine grained siliciclastic material with variable amounts of calcium carbonate.

3. Material and methods

In 2007, during cruise M72/5 of the German *RV Meteor*, six gravity cores with 12 cm diameter and lengths between 8 and 9.5 m were recovered from three water depths, down-slope along the Archangelsky Ridge in the southeastern Black Sea (Fig. 1, Supplementary Table S1). The obtained sediments were studied for their sedimentologic, paleoclimatic, paleomagnetic, and rock magnetic records.

3.1. Sedimentologic investigation

X-ray fluorescence (XRF) scanning was performed on split archive core halves at the MARUM laboratory at Bremen University, Germany, using an Avaatech XRF core scanner configured with an Amptek detector. Counts of major elements were obtained every 1–2 cm with an integration time of 15 s and an X-ray current of 0.15 mA (Röhl and Abrams, 2000). The carbonate contents were determined with an EuroEA 3000 (EuroVector CHNS Elementar analysator, HEKAtech Ltd.). After freeze-drying and homogenization with mortar and pestle, 5 mg of sediment was used to determine total carbon (TC) and 3 mg was used to determine total organic carbon (TOC). TOC was subtracted from TC in order to obtain total inorganic carbon (TIC). The molecular-weight of C is 12.011. The molecular-weight of $CaCO_3$ is 100.086 (Ca=40.978, $3\times$O=47.997, C=12.011). Thus, TIC was multiplied by 8.333 in order to obtain the calcium carbonate content ($CaCO_3$).

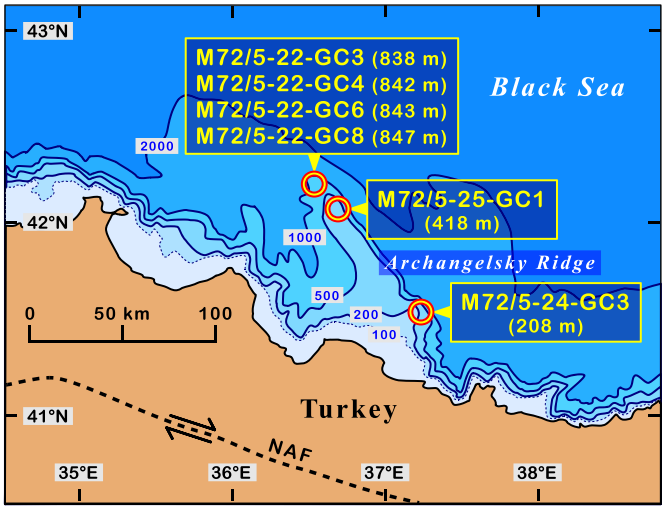

Fig. 1. Simplified bathymetric map of the southeastern Black Sea continental slope offshore of Turkey with coring sites (circles) from *RV Meteor* cruise M72/5 in 2007. Core numbers are indicated together with corresponding water depth in brackets. NAF – North Anatolian Fault.

For determination of the amount of ice-rafted detritus (IRD) sediment sub-samples (10 cm^3) were wet-sieved and particles >125 μm were counted under a light microscope. In order to make individual IRD records comparable, the following procedure was applied to each data set. Zero-counts were set to 0.1. Because log(0.1) equals -1, before normalising by the log(maximum), an offset of $+1$ was added to the log-values of both the IRD counts and their respective maximum of each core so that:

$$\log(\mathrm{IRD})_{\mathrm{norm}} = (\log(\mathrm{IRD})+1)/(\log(\mathrm{IRD}_{\mathrm{max}})+1). \quad (1)$$

Thus, values range between 0 (no IRD), representing warm phases, and 1 (maximum IRD), representing cold phases. Consequently, the log-normalised IRD records are plotted on an inverted *y*-axis.

3.2. Radiometric dating and tephra identification

For accelerator mass spectrometry (AMS) ^{14}C dating, 16 samples containing juvenile shells of the bivalve species of *Dreissenia rostiformis* were collected from core M72/5-24-GC3. The analyses were performed at the radiocarbon laboratory at the ETH/PSI facility in Zürich, Switzerland. ^{14}C ages were converted into calibrated calendar ages before present, defined as AD 1950, using the Calib 6.0 radiocarbon tools with the INTCAL09 calibration curve (Reimer et al., 2009). Microprobe analyses on manually extracted tephra particles from wet-sieved sub-samples were performed using a CAMECA SX 100 electron microprobe (15 kV voltage, 20 nA analytical current, 15 μm beam size).

3.3. Paleo- and rock magnetism

Low-field volume magnetic susceptibility (κ_{LF}) was determined with an automated core logger using a Bartington Instruments MS2E spot-reading sensor in steps of 1 mm on the split surface of the working halves of the cores. The cores were then sampled with cubic plastic boxes (internal size $2.0\times2.0\times1.6$ cm) at a standard distance (centre to centre) of 2.5–3.0 cm (Supplementary Table S1). Preliminary stratigraphic results from XRD and magnetic susceptibility scanning allowed identification of oxygen isotope stage 3, which was then mostly (re-) sampled with a high-resolution scheme with 45°-rotated boxes in two parallel rows at an offset of half a sample's diagonal (see inset in Fig. 2b), yielding a total of 2287 samples.

Measurements and stepwise demagnetisation of the natural remanent magnetisation (NRM) of all discrete samples were performed with a 2G Enterprises 755 SRM long-core magnetometer with an in-line tri-axial alternating field (AF) demagnetiser, adapted for synchronous measurement of 8 discrete samples. Peak AFs of 0, 5, 10, 15, 20, 30, 40, 50, 65, 80 and 100 mT were used to identify the stable NRM directions and to remove secondary viscous overprints. In general, successive measurements after AF demagnetisation from 15 to 65 mT were used to determine the characteristic remanent magnetisation (ChRM), using principal component analysis (Kirschvink, 1980). The cores were not oriented, therefore ChRM declinations were simultaneously rotated to a common mean value of 0°. For this purpose, a circular window of 35° radius around the expected dipole inclination of 61° was used to exclude directions related to non-dipolar field geometries, and reversed directions were recalculated to normal polarity. Data were rotated until all ChRM directions falling into this circular window yielded a Fisher (1953) mean of 0° declination. The obtained declination correction was applied to all samples of a core. Directional data after this simple declination correction are shown as red curves in Fig. 2. In data from some cores, a slight drilling-induced twisting of ChRM declination was observed. In such cases, all ChRM declination values falling into a window around the dipole direction with $\pm 35^\circ$ in inclination and $\pm 45^\circ$ in declination, were used for a trend correction by linear regression (black curves in Fig. 2).

An anhysteretic remanent magnetisation (ARM) was imparted to discrete samples with a separate 2G Enterprises 600 single-axis AF demagnetiser, with an AF of 100 mT and a superimposed direct current (DC) field of 0.05 mT was generated by an integrated DC coil. Measurements and stepwise demagnetisation were performed with the long-core magnetometer at AF steps of 0, 10, 20, 30, 40, 50, and 65 mT in order to determine the median destructive field (MDF), and to provide data for estimation of relative paleointensity (RPI) variations using ARM normalisation. The latter was always calculated using the NRM/ARM intensity ratio after application of AF demagnetisation at 30 mT each.

An isothermal remanent magnetisation (IRM) was imparted using a 2G Enterprises 660 pulse magnetiser. IRM intensities acquired in a peak field of 1.5 T are defined as the saturation IRM (SIRM). Analog to Bloemendal et al. (1992), a reversed field of −0.2 mT was used to determine the S-ratio, defined here as:

$$S = 0.5 \times \left(1 - \left[\mathrm{IRM}_{-0.2\,\mathrm{T}}/\mathrm{SIRM}_{1.5\,\mathrm{T}}\right]\right), \text{ with } 0 \le S \le 1. \quad (2)$$

Values close to 1 indicate the dominance of low coercivity minerals such as magnetite (Fe_3O_4) and Greigite (Fe_3S_4), whereas values close to 0 indicate the dominance of high coercivity minerals such as hematite (Fe_2O_3) and goethite (FeOOH). A total of 85 measurements of saturation magnetisation versus temperature, obtained with a Variable Field Translation Balance (VFTB), were used to identify the Curie-temperature (T_C) of the magnetic carriers. Measurements of saturation magnetisation (M_S) were performed on moist sediments in argon at a field of 525 mT, almost directly after finishing IRM investigations.

3.4. Tuning procedure

A special graphics program, the e**x**tended **t**ool for **c**orrelation (**xtc**, Linux-based) developed at the GFZ Potsdam, Germany, was used for tuning. **xtc** facilitates simultaneous handling of data from several cores with up to 12 parameters in common by using an interactive wiggle-matching routine. The six data sets were simultaneously tuned in detail to the GICC05 time scale of the North Greenland Ice core Project (NGRIP) $\delta^{18}O$ reference record (Svensson et al., 2006, 2008) back to 60 ka. There is a striking similarity of some Black Sea sedimentary parameters with the oxygen isotope record from Greenland ice cores, therefore, no phase lag was assumed between the two paleoclimatic records. By parallel tuning of climate-related variations in Black Sea records of log-normalised IRD abundances, carbonate content, Ca XRF-counts, and high-resolution magnetic susceptibility, simultaneous synchronization of the associated paleomagnetic records, ChRM inclination and declination and relative paleointensity, could be achieved.

Fleitmann et al. (2009) present high-resolution oxygen and carbon isotope analyses on stalagmites from NW-Anatolia, Turkey, that also resemble the pattern of rapidly alternating high-latitude cooling and warming events, the so-called Dansgaard–Oescher (D–O) events (Dansgaard et al., 1993). Numerous ages based on ^{230}Th dating differ by up to several hundreds of years from ages given in the GICC05 age model for the D–O events. However, especially around 40 ka, at the time of the Laschamp excursion these deviations are small, in the range of 0.0 kyr (D–O8) to 0.8 kyr (D–O 11 and 12). Therefore, but mainly because we have to relate our data to other GICC05-based data, we prefer to stay with the GICC05 chronology and not to adopt ages from Fleitmann et al. (2009) to the studied Black sea sediments.

The **xtc** software also allows stacking of a selected physical property, including ChRM directions (paired inclinations and declinations) into time series with a constant sampling rate. In general, because of the high data density, data were gathered into bins of 20 yr. Arithmetic averages were calculated for normalised IRD counts, carbonate contents, Ca XRF-counts, and magnetic susceptibility. Since secondary magnetic iron sulphides are generally characterized by higher susceptibility values, data points exceeding 450×10^{-6} (SI) were omitted during stacking. Fisher (1953) statistics were used to determine mean paleomagnetic directions and the α_{95} angle of confidence, using paired ChRM inclinations and declinations from cores from site M72/5-22. Subsequent calculation of VGPs, including the error oval (dp,dm), is based on these Fisherian mean directions.

4. Results

4.1. Magnetic properties

Major magnetostratigraphic results, down-core plots of ChRM inclination and declination, relative paleointensity, S-ratio, and the SIRM/κ_{LF} ratio from the studied cores are shown in Fig. 2. Red curves represent complete (raw) data sets whereas black curves represent final data sets filtered from the effects of secondary magnetic iron sulphides (see below). Directional data for all 6 cores exhibit typical secular variation patterns. In addition, evidence for the Laschamp geomagnetic excursion (e.g., Bonhommet and Babkine, 1967; Guillot et al., 1979, Plenier et al., 2007) can be seen mainly in cores from site M72/5-22 (Fig. 2c–f) characterised by fully reversed directions. The main directional variability of the Laschamp event is bracketed by the lowest paleointensities estimated for the studied sediment records. Core M72/5-24-GC3 records a pronounced declination swing at ~35 ka (Fig. 2a). This is interpreted as an expression of the Mono Lake excursion (Denham and Cox, 1971; Liddicoat and Coe, 1979; Lund et al., 1988; Laj and Channell, 2007; Kissel et al., 2011).

Vector end point diagrams from AF demagnetisation results from across the Laschamp excursion in core M72/5-22-GC8 are shown in Fig. 3. AF demagnetisation at 10 to 15 mT was typically sufficient to isolate the stable ChRM direction from a small viscous overprint. With progressing demagnetisation, vector end points migrate toward the origin of the vector end point diagrams. Plots of the vertical component versus the horizontal component (instead of the N or E component) were chosen in order to directly visualise the inclination together with the declination (North vs. East). Their stratigraphic context is shown in the zoomed-in down-core plot in the lower right-hand side of Fig. 3.

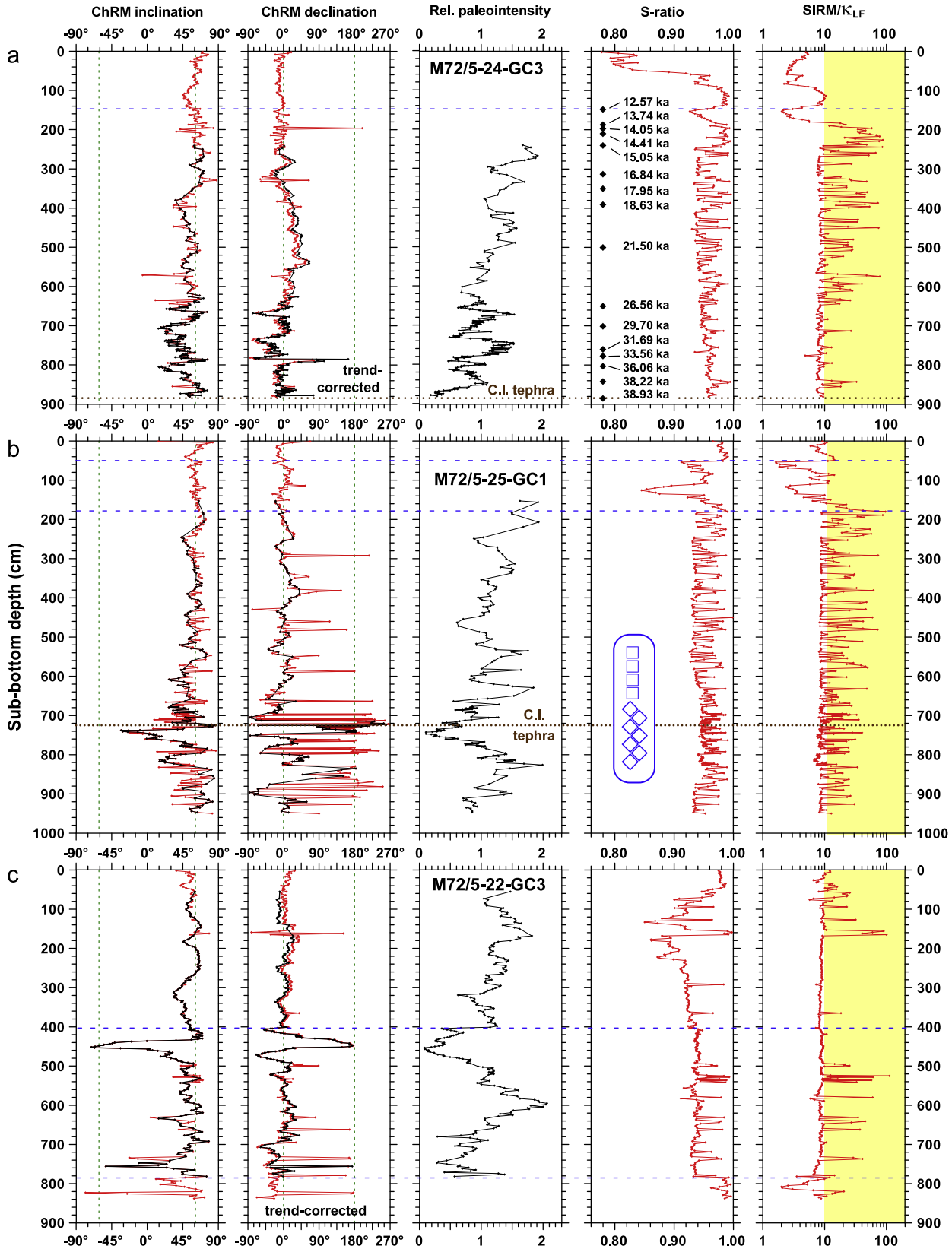

Fig. 2. Down-core plots of paleo- and rock magnetic properties: ChRM inclination and declination, with: red=raw data, black=iron sulphide-filtered data, normalized relative paleointensity based on NRM/ARM after AF demagnetisation at 30 mT after filtering for iron sulphides, S-ratio, and SIRM/κ_{LF}. All samples with SIRM/$\kappa_{LF} > 10$ kAm^{-1} and S-ratios > 0.95 were interpreted as being contaminated by secondary iron sulphides and, therefore, were excluded from further processing of paleomagnetic data. Horizontal dashed blue lines indicate inferred hiatusses, dotted horizontal brown lines marks the position of tephra material related to the Campanian Ignimbrite (C.I.) (De Vivo et al., 2001; Pyle et al., 2006). Vertical dashed lines in the inclination and declination plots indicate the expected dipole direction for normal ($I=+61°$, $D=0°$) and reversed ($I=-61°$, $D=180°$) polarity at the latitude of the coring sites. ChRM – characteristic remanent magnetisation, NRM – natural remanent magnetisation, ARM – anhysteretic remanent magnetisation, SIRM – saturation isothermal remanent magnetisation, κ_{LF} – low-field volume magnetic susceptibility. Ages in (a) in the S-ratio plot for core M72/5-24-GC3 indicate accelerator mass spectrometry (AMS) ^{14}C datings (see also Supplementary information). The blue inset in (b) in the S-ratio plot for core M72/5-25-GC1, illustrates the two different sampling schemes applied to the cores: single column squares – standard sampling, double column diamonds – high-resolution sampling. Open black diamonds in (f), in the down-core plot of SIRM/κ_{LF} for core M72/5-22-GC8, mark samples with thermomagnetic data shown in Fig. 4.

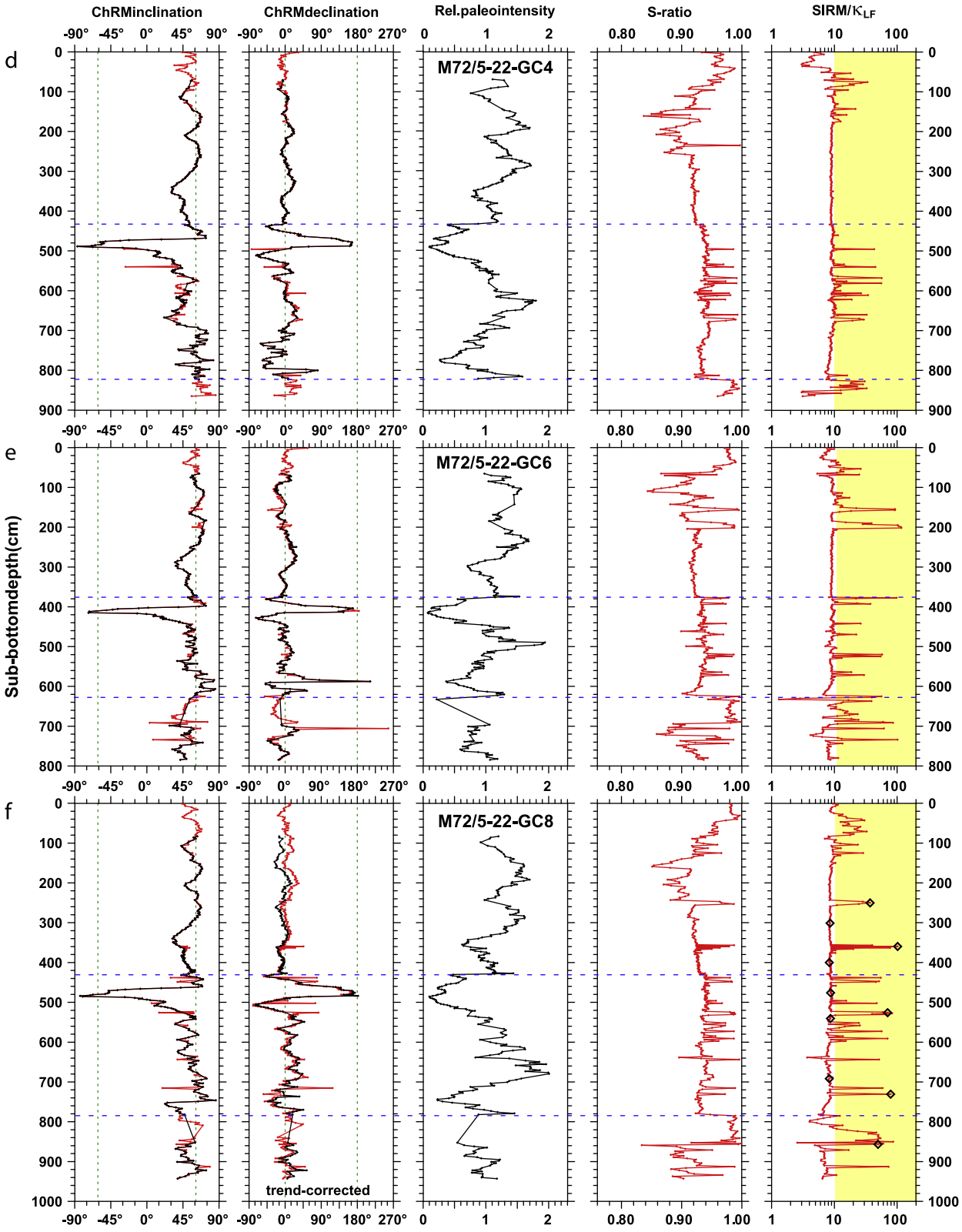

Fig. 2. (*continued*)

Magnetic properties of the sediments from the deepest coring site (M72/5-22, Fig. 1) are dominated by detrital magnetite, which is interpreted as the primary magnetic phase, with only minor to moderate variations (factor of 3) in both grain size (e.g. SIRM/ κ_{LF}, Fig. 2) and concentration. Diagenetically formed secondary iron sulphides, in general greigite, are restricted to certain horizons and to some black mottled intervals. Representative thermomagnetic results from 10 samples from core M72/5-22-GC8 are shown in Fig. 4, which illustrate the presence of magnetite (Fe_3O_4, $T_C \sim 580$ °C, e.g., Fig. 4e, g) and greigite (Fe_3S_4, disintegrating between 280 and 400 °C, Roberts, 1995; Fig. 4c, i, j). The stratigraphic positions of these samples are marked by black diamonds in Fig. 2f. In Fig. 4j,

pyrrhotite (Fe_7S_8) can be recognized from its Curie-temperature of ~320 °C in the cooling curve (blue), but very likely pyrrhotite formed out of pyrite through baking out of sulphur. This is confirmed by VFTB and Kappabridge measurements of a pure pyrite sample (in argon). As can be seen from Fig. 2, there are many single samples largely deviating in direction from their adjacent samples. In all cases, these samples are characterized by a high SIRM/κ_{LF} ratio, indicating a significant content of secondary magnetic iron sulphides (e.g., Snowball and Thompson, 1990; Snowball, 1991; Roberts and Turner, 1993; Reynolds et al., 1994; Ron et al. 2007). Since the age of the secondary magnetic iron sulphides is unknown, probably several thousands of years younger than the surrounding sediments (e.g. Rowan et al., 2009), these samples were filtered out for further processing. In the studied Black Sea sediments, sulphide bearing samples determined from thermomagnetic analyses are typically characterised by SIRM/κ_{LF} ratios $\gg 10\ kAm^{-1}$, sometimes reaching values of 50 to 100 kAm^{-1}. Samples devoid of sulphides are characterised by values of 5 to $<10\ kAm^{-1}$ (Figs. 2 and 4). Therefore, a SIRM/κ_{LF} cut-off of 10 kAm^{-1} was defined to exclude paleomagnetic data from samples contaminated with sulphides (yellow areas in Fig. 2). The limnic unit from the deepest coring site (M72/5-22), about at a depth of approximately below 50 cm, is least contaminated with sulphides compared with the intermediate and shallow water depth sites (M72/5-25 and M72/5-24), where up to 75% of the paleomagnetic data were omitted, especially from sediments directly underlying the Holocene sapropelitic sediments. Secondary sulphide formation after (assumed) partial dissolution of primary iron oxides is interpreted as the main reason why only a suppressed expression of the Laschamp excursion could be obtained from core M72/5-25-GC1. Sulphide-bearing samples are also characterised by S-ratios >0.95 (Fig. 2). Therefore, in addition, samples with S-ratios >0.95 were additionally excluded from further interpretation. This is important in cases where the magnetic susceptibility (κ_{LF}) is so low that paramagnetic contributions introduce a significant bias to the SIRM/κ_{LF} ratio. Furthermore, all Holocene samples were excluded. In Fig. 2 the unfiltered data sets (ChRM directions, SIRM/κ_{LF} ratios, S-ratios) are plotted in red, whereas the final sulphide-filtered directional data (with additional declination corrections by linear regression, when necessary because of core twisting), and normalised relative paleointensities (NRM/ARM ratios after demagnetisation at 30 mT) are plotted in black. Only these data sets were used for further paleomagnetic interpretation.

4.2. Sedimentology and dating

The glacial limnic sediments generally consist of fine-grained siliciclastic material with variable amounts of calcium carbonate. Such inorganically-precipitated carbonates have been described in the Black Sea for the late glacial Bølling–Allerød and early Holocene warming (Bahr et al., 2005; Kwiecien et al., 2008) and appear also as distinct peaks in carbonate content and Ca counts from XRF scanning data in the earlier part of the glacial period. A typical process in lakes that causes authigenic carbonate precipitation is CO_2-assimilation and pH-increase by phytoplankton blooms during warm periods (Bahr et al., 2005). Increased carbonate content causes a moderately decrease in the amplitudes of magnetic susceptibility measured down-core. Bulk grain size analyses on the sediment cores revealed the presence of large (up to 7 mm), well-rounded detrital particles in the fine-grained sediment matrix. We interpret these as ice rafted detritus (IRD) deposits that indicate the formation of coastal winter ice along the southern Black Sea margin during cold periods of the last glacial. Coastal ice formation and its subsequent drifting and melting have been identified as significant erosional processes responsible for offshore sediment displacement in larger lake basins (Kempema et al., 2001). We observe IRD abundances to increase toward the coast and high IRD counts are concentrated in time intervals where inorganically-precipitated carbonates (representing warm periods) are absent in the sediment cores.

The initial stratigraphy of the sediment cores is based on a sequence of 16 bivalve AMS ^{14}C ages from core M72/5-24-GC3, which span the time interval from 12.5 to 38.9 ka cal. BP (Fig. 2a; Supplementary Table S2). Subsequently, calcium carbonate content records (2 cores), calcium XRF-counts (4 cores), and IRD records (2 cores), representing the succession of Black Sea warm and cold intervals, could be tuned precisely to the NGRIP oxygen isotope record (Andersen et al., 2006; NGRIP members, 2004; Svensson et al., 2006, 2008) from 30 ka back to 60 ka. Cores lacking these data were finally synchronised using their high-resolution magnetic susceptibility records, as a common parameter from all cores. The result of this correlation is shown in Fig. 5, which includes relative paleointensity, as an example of the simultaneously synchronized paleo- and rock magnetic records. The investigated Black Sea sediments, like Turkish stalagmites (Fleitmann et al., 2009) clearly recorded the pattern of rapidly alternating cooling and warming of the D–O events. The paleoclimatic aspects of these results will be discussed elsewhere. AMS ^{14}C ages and tuning of Black Sea data to NGRIP resulted in the age models shown in Fig. 6a.

Further age information is provided by marker tephras that were detected within the studied southeastern Black Sea sediment cores. The average major element composition of glass shards from the distinctly visible tephra layer can be related to the distal ash fall associated with the Campanian Ignimbrite (De Vivo et al., 2001; Pyle et al., 2006), which we hereafter refer to as C.I. tephra (also known as the Y5 tephra). Samples from cores M72/5-24-GC3 (882 cm) and M72/5-25-GC1 (721 cm), marked by dashed lines in Fig. 2, contain a population of glasses (Fig. 6b and c) that is compositionally similar to various proximal to mid-distal pyroclastic density current (PDC) deposits of the C.I. tephra (Giaccio et al., 2008; Supplementary Table S3). For comparison, Fig. 6b and c include further geochemical data for the C.I. tephra from Italy (Wulf et al., 2004), Macedonia (Wagner et al., 2008), and Greece (Müller et al., 2011). In two of the cores (M72/5-24-GC3, M72/5-25-GC1), electron microprobe analyses also confirm the presence of the Y2 Santorini tephra (not shown, Kwiecien et al., 2008). The Campanian Ignimbrite erupted from the modern Campi Flegrei, Italy, at 39.28 ± 0.11 ka BP (De Vivo et al., 2001) and our coring sites are located at the postulated easterly geographical limit of preservation of the visible C.I. tephra (see Fig. 1 in Pyle et al., 2006). According to the derived age models of the Black Sea cores, the C.I. tephra is placed between D–O8 and D–O9 at 39.4 ka BP, which is in good agreement with radiometric dating (De Vivo et al., 2001).

According to Fig. 6a, at sites M72/5-24 and M72/5-25 sedimentation rates are in the range 12–15 cm kyr^{-1} and the records reach back 39.4 ka BP and 63 ka BP, respectively. Cores from site 22 contain two major hiatuses from about 20 ka to 39.4 ka BP, and from about 68 to 118 ka BP (not discussed here), but the interval in between has sedimentation rates up to 25 cm kyr^{-1}, especially around 40 to 45 ka BP. The late glacial is characterised by sedimentation rates that reach up to about 60 cm kyr^{-1}. The hiatuses at the studied sites are likely caused by slumps that were triggered by major earthquakes along the North-Anatolian fault close to the coring sites (Fig. 1).

4.3. Chronostratigraphy

The synchronised and subsequently stacked records (arithmetic means in 20 yr bins) of IRD, calcium carbonate content, calcium XRF-counts, and high-resolution magnetic susceptibility, together with individual records of ChRM inclination and declination from the studied Black Sea sediments are shown in Fig. 7, along with the NGRIP ice core $\delta^{18}O$ record and numbered D–O events. The four ChRM inclination and declination records from

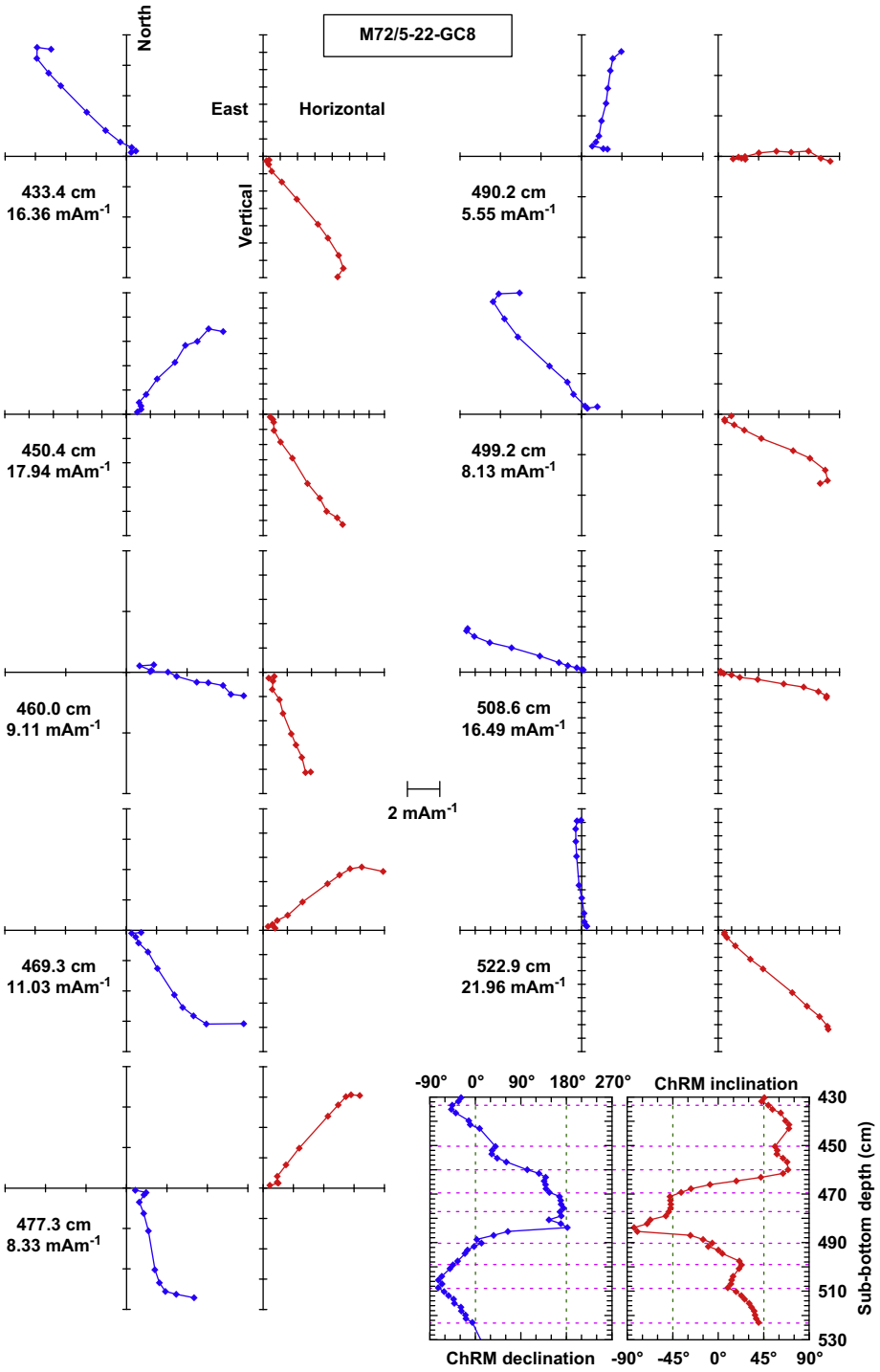

Fig. 3. Paleomagnetic directional variations for 9 samples across the Laschamp excursion during the course of alternating field demagnetisation (core M72/5-22-GC8). Results are shown as vector end point diagrams in the horizontal (N vs. E) plane (declination, blue) and the associated vertical (Z vs. H) plane (inclination, red). Positions of the samples are marked by horizontal dashed lines in the down-core plots of ChRM inclinations and declinations in the lower right. ChRM – characteristic remanent magnetisation.

site M72/5-22 are in excellent agreement, with consistent indications of a full reversal of the local field vector. Results from core M72/5-25-GC1 are hampered by massive precipitation of secondary magnetic iron sulphides (Fig. 2b) and core M72/5-24-GC3 covers only the past 39.4 ka (Fig. 2a and 6a) we, therefore, concentrate mainly on data from site M72/5-22. The high-resolution sampling and reproducibility of the data from these four parallel cores allows stacking of the directional data (ChRM inclination and declination) into 20 yr bins using Fisher (1953) statistics. From this stack, the corresponding VGP positions were calculated for the time interval from 43.0 to 39.4 ka, which spans the Laschamp excursion (Fig. 8). Within that period, six mean directions were calculated individually for time windows when the VGPs persisted spatially, independent from stacking into 20 yr bins. The corresponding VGPs and error ovals of these six separate calculations are labelled and plotted in red in Fig. 8 (Roman numerals). VGP latitudes and paleointensities from the site M72/5-22 stack are shown over a longer time window reaching back to 50 ka in Fig. 9 together with both the oxygen isotope record (Svensson et al., 2006, 2008) and the ^{10}Be record (Muscheler et al.,

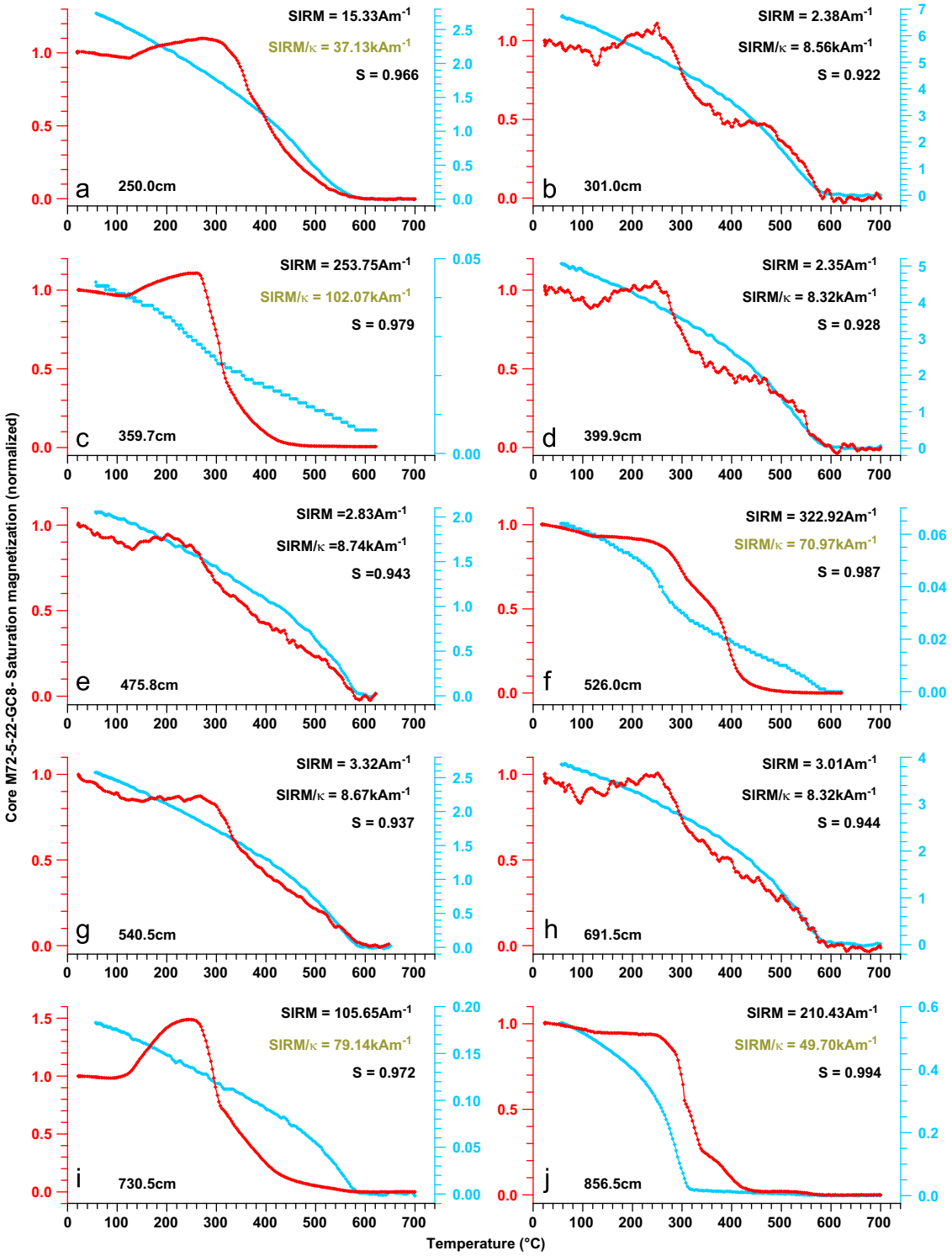

Fig. 4. Thermomagnetic curves from selected samples from core M72/5-22-GC8, marked by black diamonds in Fig. 4f. Samples containing significant amounts of magnetic iron sulphides are generally characterised by SIRM/κ_{LF} ratios $\gg 10$ kAm^{-1}. Red (blue) indicates the heating (cooling) curve. Note: for reasons of clarity, heating and cooling curves are scaled separately. SIRM – saturation isothermal remanent magnetisation, κ_{LF} - low field volume magnetic susceptibility. S – S-ratio (see text for definition).

2004) from Greenland ice cores. Inferred durations of excursional field features are estimated on the basis of the high-resolution age model described above.

VGP data and relative paleointensities from core M72/5-24-GC3, together with both the oxygen isotope record (Svensson et al., 2006, 2008) and the ^{10}Be record (Muscheler et al., 2004) from Greenland ice cores are shown in Fig. 10. Data are shown for the time window from 15 to 40 ka, which is mostly missing in cores from site M72/5-22. Several time intervals in core M72/5-24-GC3 have VGP latitudes of $\sim$45°N or less. During the oldest interval, centred at 34.5 ka, VGPs perform a wide clockwise loop across Asia, northern Africa and North America (black VGPs in Fig. 10). We interpret this feature as a recording of the Mono Lake excursion (Denham and Cox, 1971; Liddicoat and Coe, 1979; Lund et al., 1988; Laj and Channell, 2007;

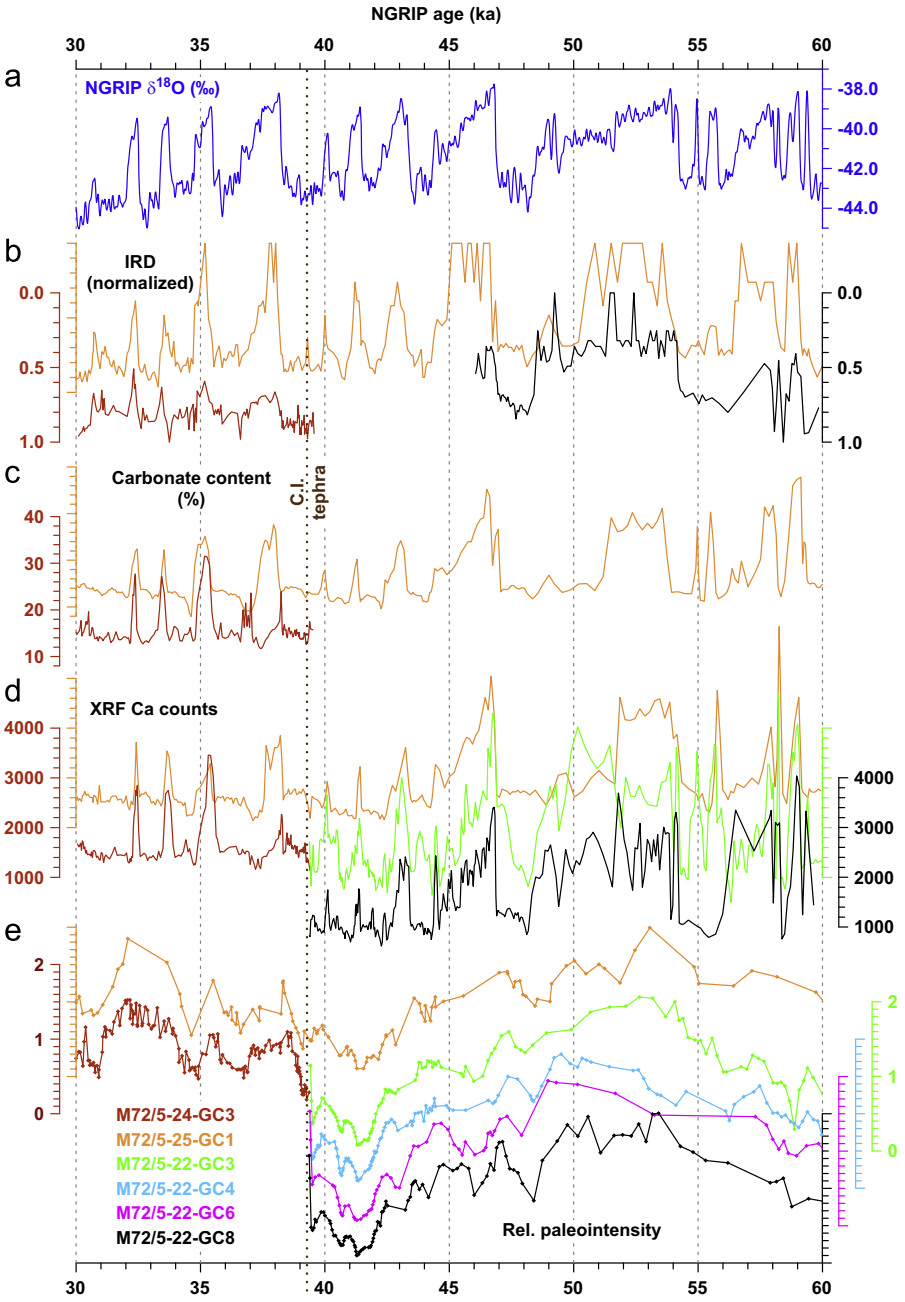

Fig. 5. (a) Oxygen isotope data from Greenland ice cores according to the GICC05 age model (Svensson et al., 2006, 2008) as reference record; (b) ice-rafted detritus (IRD); (c) bulk carbonate content; (d) XRF Ca counts; and (e) relative paleointensities (see also Fig. 2). Data are shown after simultaneous tuning to the Greenland oxygen isotope record in a). Colours of the curves and axes refer to the core numbers listed in the lower left. The dotted vertical line marks the stratigraphic position of the Campanian Ignimbrite tephra (e.g., De Vivo et al., 2001), identified in cores M72/5-24-GC3 and M72/5-25-GC1.

Kissel et al., 2011). In core M72/5-25-GC1 VGP latidues are all $>45^{\circ}$N for the time interval from 15 to 40 ka (not shown). However, reliable data from this core is sparse, because many samples were contaminated by secondary magnetic iron sulphides so that their data were removed from the paleomagnetic record.

5. Discussion

5.1. Field geometry during the Laschamp excursion

In contrast to most sedimentary records of the Laschamp excursion compiled by Laj et al. (2006), VGPs from the studied Black Sea sediments do not show a simple clockwise loop (Fig. 8). Instead, the VGP first moved from the Bering Sea via NE America to the Sargasso Sea (down to 15°N) and stayed there for about 270 yr (VGP I in Fig. 8). It then moved back across NE America to the NE Pacific at around 45°N resting there for about 300 yr (VGP II in Fig. 8) and migrating subsequently within 200 yr to the high southerly latitudes ($>70^{\circ}$S) in Antarctica. After clustering at high latitudes over two sites in the Pacific and the Indian Ocean sectors of Antarctica for a total of about 440 yr (VGPs III and IV in Fig. 8), the VGP then took about 270 yr to cross the Indian Ocean via the Himalayas to Central Siberia, residing there for 250 yr (VGP V in Fig. 8). After a short excursion lasing 250 yr, with VGPs over the Labrador Sea at about 50°N (VGP VI in Fig. 8), the VGP finally swung back to the Arctic Ocean. Thus, main directional changes of the Laschamp excursion are characterised by a short-lived but full VGP swing to reversed polarity directions, bracketed by preceding as well as succeeding (though less pronounced) excursions

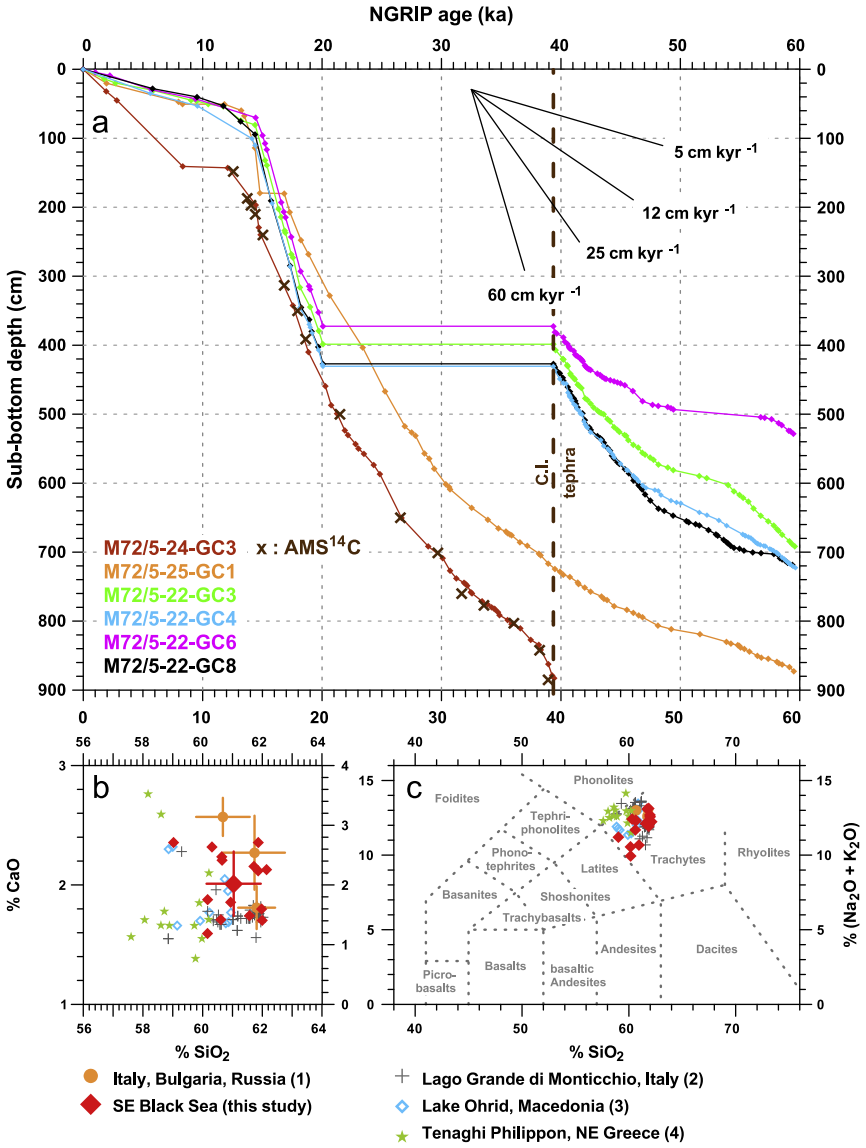

Fig. 6. (a) Age–depth curves for the investigated Black Sea sediment cores as obtained by multi-parameter tuning to the NGRIP ice core record (GICC05 age model, Svensson et al., 2006, 2008), using calibrated AMS^{14}C ages (brown crosses; see also Fig. 2a and Supplementary Table S2), and published age of the Campanian Ignimbrite (De Vivo et al., 2001), indicated by the brown dashed line, as initial tie points. Colours of the curves refer to the core numbers listed in the lower left. The fan of lines in the upper right indicate the range of sedimentation rates for the studied sediment cores. The geochemical fingerprint of tephra particles from the Black Sea related to literature data (1, Giaccio et al., 2008; 2, Wulf et al., 2004; 3, Wagner et al., 2008, 4, Müller et al., 2011) of the Campanian Ignimbrite tephra are shown in b) CaO/SiO_2-ratio and c) total alkali versus silica (TAS) diagram (right). Mean geochemical results for distal tephra sites (1) and of this study are shown with their corresponding 1σ standard deviation (see also Supplementary Table S3).

over the NW Atlantic Ocean. The maximum inferred VGP speed is in the range of half a degree in latitude per year during the transitional phase between the clear normal (N) polarity (VGP latutides $>45°$N) and the clear reversed (R) polarity (VGP latitudes $>45°$S), and back (Fig. 8). The whole duration of these complex directional variations lasted some 3000 yr (Fig. 9), with about a total of 1200 yr characterized by transitional directions (vertical grey bars in Fig. 9). Rapid directional changes during the Laschamp can also be inferred from a high-resolution record of the Laschamp excursion at the southern mid-latitute ODP Site 1233 (Lund et al., 2006).

In the marine record from the Bermuda Rise (ODP Site 1063), the Laschamp excursion has been recorded at sedimentation rates of 40 cm kyr^{-1}. There, it is characterised by a total duration of about 500 yr (Channell et al., 2012), centered at 40.8 ka, with VGPs also reaching high southern latitudes. However, within their (U-channel) record, the VGPs pass over Eastern Antarctica (Fig. 7 in Channell et al., 2012), whereas in the Black Sea record VGPs persist in Antarctica for 440 yr (total of 26 VGPs, Fig. 8). The Bermuda Rise sediments also recorded a precursor to the Laschamp excursion with VGPs reaching to about 15°N, but with a wide loop instead of VGPs moving southward and then back northward within a narrow corridor as is the case for the Black Sea VGPs. Another similarity between the two records is the short persistence of VGPs along the NW coast of North America before the N–R transition (Bermuda Rise: Alaska, USA; Black Sea: British Columbia, Canada). The observed similarities might favour the interpretation of a dominant dipolar geometry compared to those presented by Laj et al. (2006), but the VGP paths of the R–N reversal are different in longitude by 60° which indicates a non-dipolar geometry of the geomagnetic field at that time.

The VGPs of the Laschamp excursion obtained from the Black Sea pass in close proximity to individual VGP clusters obtained from the different lavas from the type locality in France (Plenier et al., 2007; Fig. 8). The closeness of these two locations, on a global scale (~25° arc length), allows correlation of the VGPs from the French lavas to the ages of the VGP positions obtained from the high deposition rate Black Sea sediments. Thus, the Laschamp/Olby flows should have

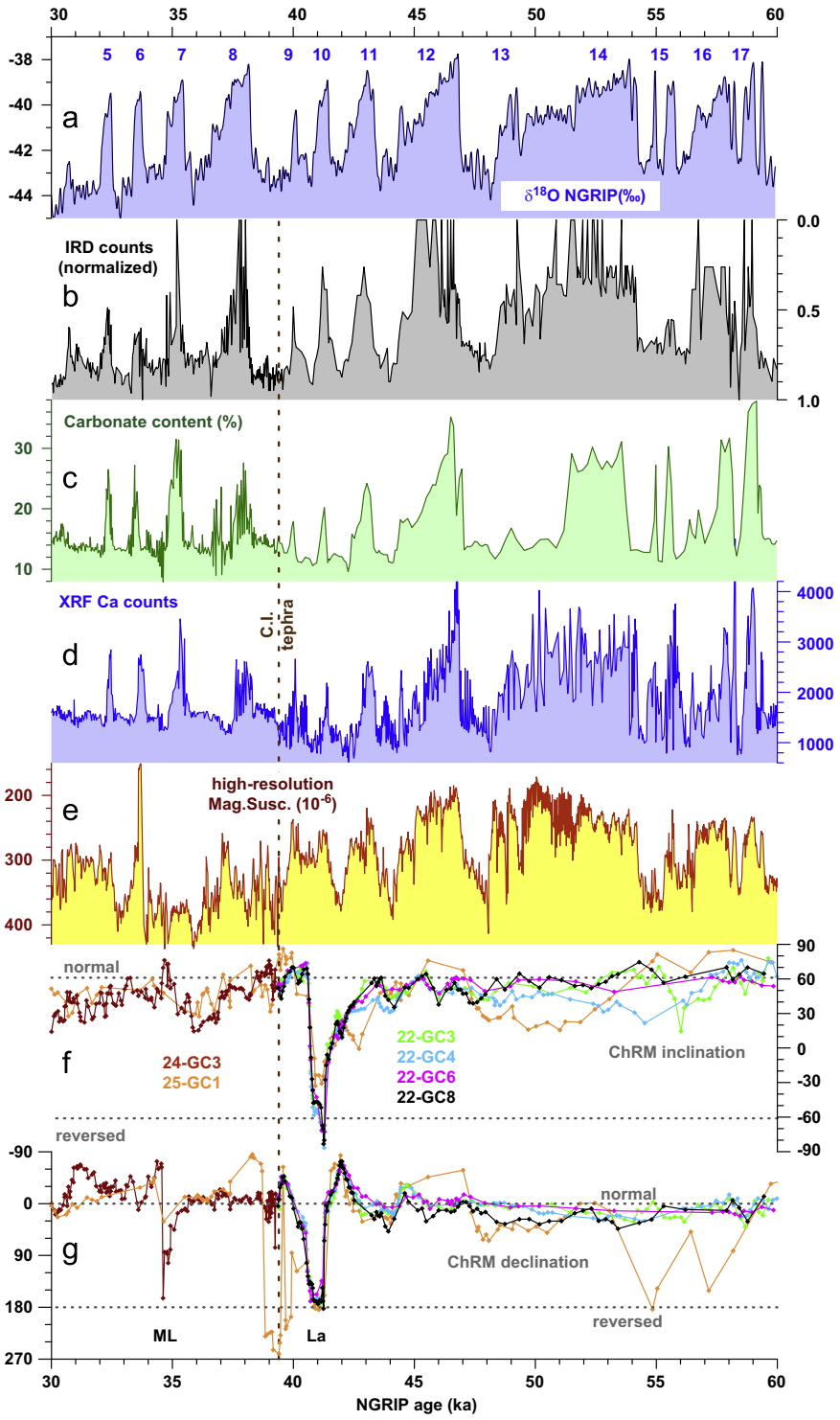

Fig. 7. (a) Oxygen isotope record according to the GICC05 age model for Greenland ice cores (Svensson et al., 2006, 2008). Numbers along the top indicate Dansgaard–Oeschger warming events (Dansgaard et al., 1993). NGRIP-tuned stratigraphic data sets from Black Sea sediments, stacked into 20 yr bins are shown for: (b) ice-rafted detritus (IRD), (c) bulk carbonate content, (d) XRF Ca counts, (e) high-resolution magnetic susceptibility, and (f) inclinations and (g) declination of the characteristic remanent magnetisations (ChRM) for the six investigated sediment cores shown as superimposed individual plots. ML – Mono Lake excursion, La – Laschamp excursion.

erupted at ~41.5 ka, just a few decades before the full reversed polarity state was reached. The intermediate directions from Louchadière, with VGPs in the northern Indian Ocean and East Africa, can be linked to the R–N transition at 40.5 ka BP. Its latest phase at 40.4 ka BP can probably be linked to the Siberian VGP from the Puy de Thiolet (Plenier et al., 2007). VGP positions from the Royat flow plot between the VGP paths of the pre- and post-reversal excursions of the Laschamp excursion from the Black Sea record (Fig. 8). Because of their closer proximity to the pre-reversal excursion and their VGP latitudes being lower than those of the post-reversal excursion from the Black Sea record, a pre-reversal age of the Royat flow can be narrowed down to between 42.2 and 41.8 ka BP (1a in Fig. 9). As a result of the largely overlapping southward and northward sections of the VGP path from the studied Black Sea sediments in that time interval, no better age assignment is possible. Alternatively, the Royat flow can be linked to the lowest VGP

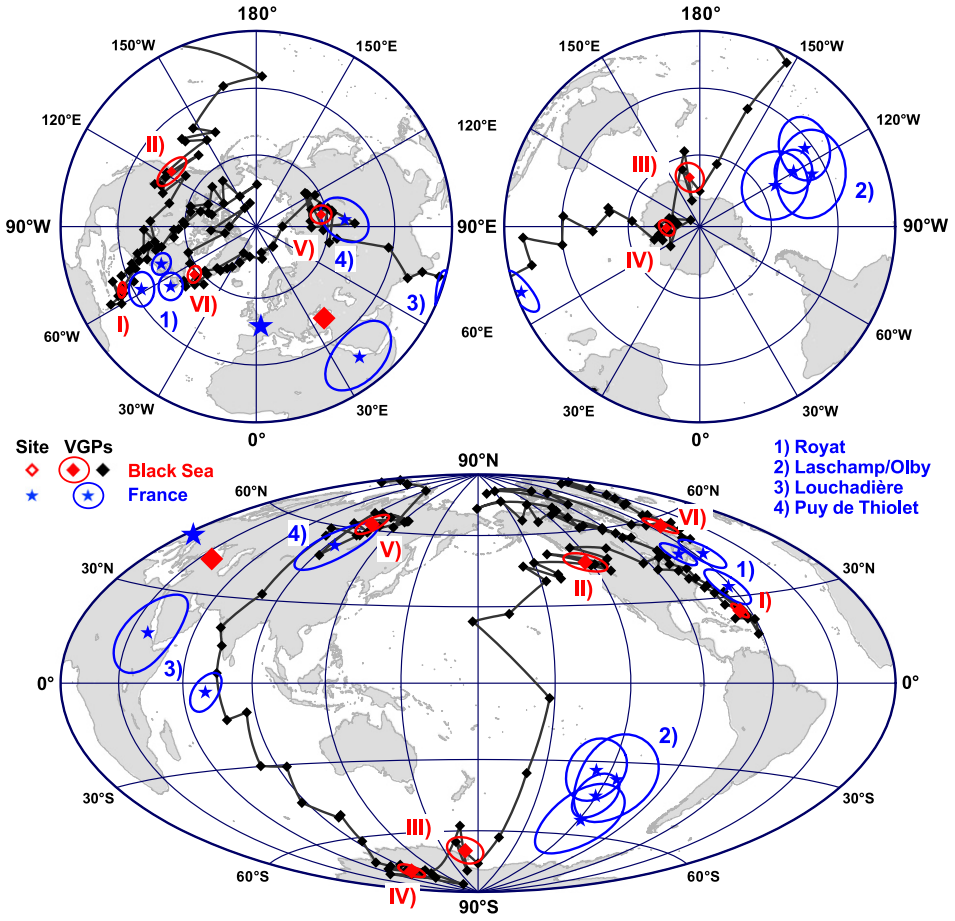

	Time interval (ka)	Incl. (°)	Decl. (°)	α_{95} (°)	n	PLAT (°N)	PLONG (°E)	dp (°)	dm (°)
I)	42.15 – 41.88	17.31	-64.02	3.0	23	25.09	295.23	1.6	3.1
II)	41.75 – 41.45	2.34	-13.73	7.2	11	47.12	236.90	3.6	7.3
III)	41.25 – 41.17	-69.77	153.43	3.7	7	-69.07	168.54	5.5	6.4
IV)	41.16 – 40.81	-52.24	167.17	2.7	19	-76.19	87.87	2.6	3.7
V)	40.54 – 40.19	65.93	38.67	2.7	19	62.42	100.56	3.6	4.4
VI)	39.72 – 39.49	54.41	-41.42	2.6	15	57.15	-52.35	2.6	3.7

Fig. 8. Averaged paleomagnetic data, Fisher (1953) means from 20 yr bins, from 4 parallel cores from site M72/5-22 for the age interval 43.0 ka to 39.4 ka. The record documents a full polarity reversal (VGP clusters III and IV) during the Laschamp excursion. Equal area projections in polar views (top) and equatorial Hammer-Eitoff projection (bottom), with VGPs connected by great circles. Age ranges and paleomagnetic data for six VGP clusters from Black Sea sediments (Roman numerals, red diamonds, and dp/dm error ovals) are listed in the lower section. Blue numbers, site names, stars, and dp/dm errror ovals indicate data from volcanic rocks of the type locality in France (e.g., Plenier et al., 2007), listed in centre-right.

latitudes of the post-reversal excursion (at around 39.6 ka; 1b in Fig. 9). Together with the other assigned ages of the French VGP positions, the latter interpretation would be consistent with an interpretation of the data from France (Valet and Plenier, 2008) that is based on a simulation of the Laschamp excursion by varying only the dipole contribution of the geomagnetic field and applying field models, such as the CALS7K.2 (Korte and Constable, 2005) for the time-varying non-dipole contributions.. In that study, the best fit of a modelled VGP path to the French lava data was obtained by decreasing the dipole to zero, reversing it for a short while with 20% of the initial field intensity, and then increasing it again to normal polarity. This model is consistent not only with the Black Sea sedimentary record in which we observe a 20% field recovery with respect to the paleointensity at 50 ka BP (Fig. 9), but also with sedimentary data from northern high latitudes (Nowaczyk, 1997; Nowaczyk et al., 2003), and, to a lesser extent with preliminary data from the SE Pacific (Lund et al., 2006), which indicate significant intensity recoveries during the reversed phase.

The directional variations of the Laschamp excursion are preceded by a gradual drop in relative paleointensity, starting at about 50 ka BP, when the geomagnetic field was strongest during the last glacial. Lowest field intensities are associated with the N–R and R–N transitional phases, with amplitudes as low as 5% of the preceding maximum at 50 ka (Fig. 9). The Black Sea relative paleointensity record is in general agreement with the global paleointensity stack (GLOPIS, Laj et al., 2004; purple dashed line in Fig. 9), when re-tuned to the NGRIP age model. However, the GLOPIS record does not include a field recovery during the time of fully reversed polarity directions during the Laschamp excursion, reaching about 20% of the intensity of the preceding intensity maximum at 50 ka BP. Such a field recovery is actually a characteristic feature of a polarity event, such as the Jaramillo event, but with a much shorter duration, supporting the idea that excursions are aborted polarity intervals, bracketed by two reversals (Valet et al., 2008).

5.2. A link to climate?

In Fig. 9 we show the NGRIP oxygen isotope record (Svensson et al., 2006, 2008) and the associated ^{10}Be record (Muscheler et al., 2004) to illustrate the enhanced production of cosmogenic radionuclides during the Laschamp excursion. Linked via their paleoclimatic records the Greenland ice core data and the Black Sea sediment data can be directly compared. There is a striking similarity between the Black Sea relative paleointensity record

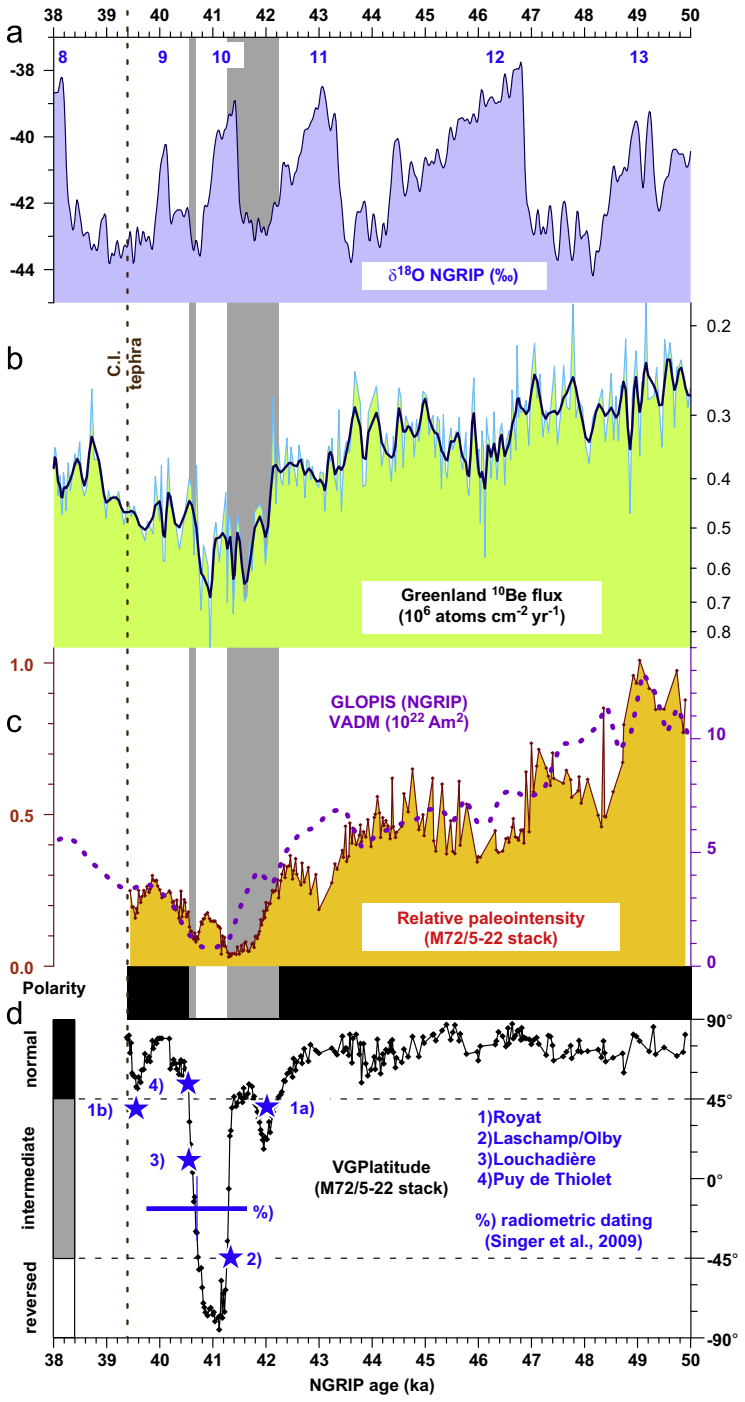

Fig. 9. (a) Greenland oxygen isotope record (NGRIP) according to the GICC05 age model (Svensson et al., 2006, 2008), with numbers at the top indicating Dansgaard–Oeschger warming events (Dansgaard et al., 1993), and (b) ^{10}Be flux (Muscheler et al., 2004), dark blue: 5 point weighted running average, together with (c) the normalized Black Sea relative paleointensity stack (20 yr bins), and (d) corresponding VGP latitudes (20 yr bins). The dotted purple line in (c) represents the global paleointensity stack (GLOPIS, Laj et al., 2004), recalculated to the GICC05 age model. VGPs above 45°N are assigned a normal polarity (black). VGPs above 45°S are assigned a reversed polarity (white). VGPs between 45°N and 45°S are defined as intermediate (grey). The blue bar marks the error range of the mean age of the French lavas from radiometric dating (Singer et al., 2009), whereas blue stars mark individual ages for the different lava flow sites in France (Plenier et al., 2007) as inferred from correlation to Black Sea data (this study, see Fig. 8). (1a): age suggested from this study, (1b) age suggested from modelling (Valet and Plenier, 2008). This data compilation illustrates the strong link between geomagnetic field intensity variations and cosmogenic radionuclide production. No direct link between climate variability and geomagnetic field intensity, as contemporaneously recorded in the Black Sea sediments is obvious from this study.

and the ^{10}Be record from Greenland. Note that the latter has been plotted with an inverted log-axis. The double maximum in Greenland ^{10}Be flux coincides with the two periods of lowest field intensity recorded in the studied Black Sea sediments (except for a 200 yr shift for the R–N polarity change), and the lower ^{10}Be flux between coincides more or less with the field recovery during the reversed polarity state of the Laschamp excursion. Two vertical grey bars in Fig. 9 indicate the transitional phases with lowest field intensities, which bracket the full reversal interval of the Laschamp excursion. An increased production of cosmogenic radionuclides, such as ^{10}Be (and also ^{14}C and ^{36}Cl; Beer et al., 2002), was first postulated by Raisbeck et al. (1985) for the Brunhes–Matuyama reversal from a sediment core from the South–west Indian Ocean. Several sedimentary records

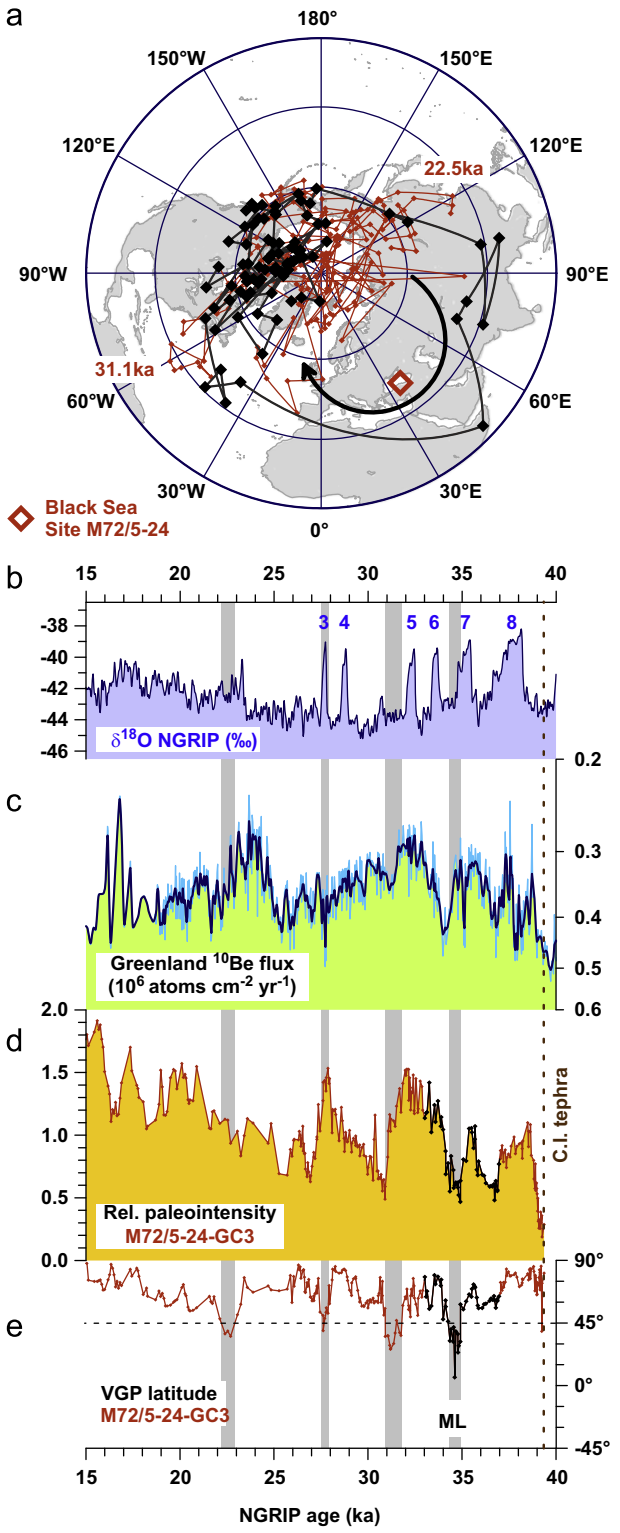

Fig. 10. (a) VGP positions obtained from core M72/5-24-GC3 (red VGP path), with VGPs from 33 to 37 ka across the Mono Lake excursion in black, performing a clockwise loop across Asia, northern Africa and North America, together with (b) the Greenland oxygen isotope record (NGRIP) according to the GICC05 age model (Svensson et al., 2006, 2008), with numbers along the top indicating Dansgaard–Oeschger warming events (Dansgaard et al., 1993), (c) ^{10}Be flux (Muscheler et al., 2004), dark blue: 5 point weighted running average, (d) the normalized relative paleointensity and (e) corresponding VGP latitudes from core M72/5-24-GC3. Grey bars in the background mark phases with VGP latitudes lower than 45°N (horizontal dashed line). ML—Mono Lake excursion. C.I.—Campanian Ignimbrite.

also provide evidence of an increased ^{10}Be flux during the Laschamp excursion (e.g., Frank et al., 1997; Christl et al., 2010) but records with the highest resolution are from ice cores (e.g., Beer et al., 2002; Muscheler et al., 2004; Raisbeck et al., 1987). Production of ^{10}Be by incident cosmic rays, interacting with atmospheric molecules in spallation processes, is mainly modulated by the strength of the solar wind, that is, the heliospheric magnetic field, and by the intensity of the geomagnetic field. The relationship is inverse, so that low (solar or geomagnetic) fields cause a high production of cosmogenic nuclides (e.g., Masarik and Beer, 1999; Beer et al., 2002), and vice versa. Cosmic rays are also suspected to have an influence on the Earth's climate (e.g., Carslaw et al., 2002). Incident cosmic particles are supposed to serve as the major cause of cloud nucleation so that higher (lower) fluxes of cosmic rays cause a slight cooling (warming) because of an increased (decreased) albedo of the Earth. Thus, the drastic decay of the geomagnetic field during the Laschamp excursion, which led to increased ^{10}Be production, could have had an impact on Earth's climate. However, climatic deteriorations during the Laschamp excursion, expressed as the rapid warming and cooling of D–O events 9 to 13 in the Greenland δ^{18}O record, are not obviously coupled to geomagnetic field variations (Fig. 9). Therefore, a general link between climate variability and geomagnetic field intensity is highly questionable.

5.3. Short note on geomagnetic field instabilities after the Laschamp excursion

Because of a long hiatus in the sedimentary record at site M72/5-22 (Fig. 6) and massive precipitation of secondary magnetic iron sulphides in core M72/5-25-GC1 (Fig. 2b) only data from single core M72/5-24-GC3 can be consulted for the time interval from 39.4 to 15 ka. Fig. 10 shows that the Laschamp excursion was followed by several short episodes characterised by VGP latitudes $<45°$N. The oldest of these episodes is coincident with a low in relative paleointensity centred at 34.5 ka and can be correlated to the Mono Lake excursion (see Laj and Channell, 2007; Kissel et al., 2011). During this excursion VGPs recorded in Black Sea sediments perform a wide clockwise loop across Asia, northern Africa, and North America, with a single VGP reaching nearly equatorial latitude. This is partly in agreement with other records, partly not (see Fig. 10 in Kissel et al., 2011). Black Sea data together with other data favour a non-dipolar field geometry during the Mono Lake excursion. However, the Black Sea data are based on a single core.

There is some discussion that the excursion recorded at its type locality, the Mono Lake Basin in North America, is actually the Laschamp excursion (e.g. Cassata et al., 2010; Cox et al., 2012; Kent et al., 2002; Zimmerman et al., 2006)). However, it is clear from other sediment records, e.g. ODP Site 919, Irminger Basin (Channell, 2006), and volcanic rocks, e.g., on Hawaii (Teanby et al., 2002), Tenerife (Kissel et al., 2011) and in the Auckland Volcanic Field, New Zealand (Cassidi and Hill, 2009; Cassata et al., 2008) that there was a geomagnetic excursion after the Laschamp at ~33 ka, which is only slightly younger in age than the excursion recorded in the studied Black Sea sediments.

Simple N–S–N excursions of the VGP to latitudes $<45°$N are recorded at ~31.1 ka and ~22.5 ka, with a less pronounced ($>45°$N) excursion at ~27.5 ka in core M72/5-24-GC3. Except for the youngest feature, which is not well recorded, these excursions are also linked to paleointensity lows, but directional deviations are largest during the preceding intensity decays. Probably, similar features were observed in Mono Lake sediments as described by Lund et al. (1988), which they refer to a recurring geomagnetic field behaviour (although ages given by Lund et al. (1988) for the Mono Lake excursion are obsolete now, see, e.g. Laj and Channell, 2007; Kissel et al., 2011).

There is a similar link between relative geomagnetic field intensity and cosmogenic radionuclide production in the time interval from 25 to 40 ka (Fig. 10c and d), as it is the case for the time around the Laschamp excursion (Fig. 9b and c). For sediments younger than 25 ka the link is less well expressed. However, with ages getting younger this interval is hampered by an increasing amount of secondary magnetic iron sulphides in core M72/5-24-GC3 (Fig. 2a) which was therefore not sampled at high resolution.

6. Conclusions

High-quality magneto-chronostratigraphic results from Black Sea sediments provide important insights into the spatial and temporal dynamics of the geomagnetic field during the Laschamp excursion. The new data classify the directional changes of the Laschamp excursion as a short (440 yr) but full reversal at around 41 ka, associated with rapid VGP (latitudinal) changes in the range of half a degree per year, and large-scale intensity variations of 20:1 when looking at a wider time frame back to 50 ka BP. Dating of the Laschamp excursion derived from Black Sea sediments is in excellent agreement with radiometric ages (Singer et al., 2009) for the French lavas at the type locality (40.70 ± 0.95 ka BP), and other marine records from the southeast Pacific (Lund et al., 2006) and North Atlantic (Channell et al., 2012). Moreover, individual VGPs from the type locality are located close to sections of the Black Sea VGP path, which makes it possible to place VGPs from the French volcanics into chronological order, which has not been achieved unambiguously by radiometric dating (Singer et al., 2009). Finally, the Black Sea record provides, for the first time, a clear and direct stratigraphic context of the Campanian Ignimbrite tephra, which resulted from the largest volcanic eruption in the Mediterranean area over the past 200 kyr (De Vivo et al., 2001) together with the Laschamp excursion, which is the most prominent geomagnetic feature in the past 100 kyr, relative to the Dansgaard–Oeschger climatic oscillations during the last glacial cycle within a single sedimentary archive. In addition, investigation of Black Sea sediments confirm the Mono Lake excursion at his location with a NGRIP/AMS ^{14}C age of $\sim$34.5 ka, low relative paleointensities, and a wide clockwise VGP loop across Asia, northern Africa, and North America.

Acknowledgements

We thank R. Muscheler for providing ^{10}Be flux data from Greenland and C. Laj for providing the GLOPIS75 data set. We thank U. Röhl who enabled access to the XRF facility at the MARUM, Bremen, Germany. T. Moldenhawer, K. Möller, M. Duwe and D. Ulbricht helped during laboratory work. We finally thank the captain and crew of *RV Meteor* for the success of cruise M72/5. We also appreciate the constructive reviews by A.P. Roberts and a second, anonymous reviewer. This work was partly funded by the German Research Foundation (Deutsche Forschungsgemeinschaft, DFG) and the Gary Comer Science and Education Foundation, USA.

Appendix A. Supporting information

Supplementary data associated with this article can be found in the online version at http://dx.doi.org/10.1016/j.epsl.2012.06.050.

References

Andersen, K.K., Svensson, A., Rasmussen, S.O., Steffensen, J.P., Johnsen, S.J., Bigler, M., Röthlisberger, R., Ruth, U., Siggaard-Andersen, M.-L., Dahl-Jensen, D., Vinther, B.M., Clausen, H.B., 2006. The Greenland Ice Core Chronology 2005, 15–42 ka. Part 1: constructing the time scale. Quat. Sci. Rev. 25, 3246–3257.

Badertscher, S., Fleitmann, D., Cheng, H., Edwards, R.L., Göktürk, O.M., Zumbuhl, A., Leuenberger, M., Tüysüz, O., 2011. Pleistocene water intrusions from the Mediterranean and Caspian seas into the Black Sea. Nature Geosci 4, 236–239.

Bahr, A., Lamy, F., Arz, H., Kuhlmann, H., Wefer, G., 2005. Late glacial to Holocene climate and sedimentation history in the NW Black Sea. Mar. Geol 214, 309–322.

Bloemendal, J., King, J.W., Hall, J.R., Doh, S.-J., 1992. Rock magnetism of late Neogene and Pleistocene deep-sea sediments: relationship to sediment source, diagenetic processes, and sediment lithology. J. Geophys. Res. 97, 4361–4375.

Beer, J., Muscheler, R., Wagner, G., Laj, C., Kissel, C., Kubik, P.W., Synal, H.A., 2002. Cosmogenic nuclides during Isotope Stages 2 and 3. Quat. Sci. Rev. 21, 1129–1139.

Bleil, U., Gard, G., 1989. Chronology and correlation of Quaternary magnetostratigraphy and nannofossil biostratigraphy in Norwegian-Greenland Sea sediments. Geol. Rundschau 78, 1173–1187.

Bonhommet, N., Babkine, J., 1967. Sur la présence d'aimantation inversée dans la Chaîne des Puys. C.R. Acad. Sc. Paris 264, 92–94.

Carslaw, K.S., Harrison, R.G., Kirkby, J., 2002. Cosmic rays, clouds, and climate. Science 298, 1732–1737.

Cassata, W.S., Singer, B.S., Cassidy, J., 2008. Laschamp and Mono Lake geomagnetic excursions recorded in New Zealand. Earth Planet. Sci. Lett. 268, 76–88.

Cassata, W.S., Singer, B.S., Liddicoat, J.C., Coe, R.S., 2010. Reconciling discrepant chronologies for the geomagnetic excursion in the Mono Basin, California: Insights from new ^{40}Ar/^{39}Ar dating experiments and a revised relative paleointensity correlation. Quat. Geochron 5, 533–543.

Cassidi, J., Hill, M.J., 2009. Absolute palaeointensity study of the Mono Lake excursion recorded by New Zealand basalts. Phys. Earth. Planet. Inter 172, 225–234.

Chauvin, A., Duncan, R.A., Bonhommet, N., Levi, S., 1989. Paleointensity of the Earth's magnetic field and K-Ar dating of the Louchadière volcanic flow. Geophys. Res. Lett. 16, 1189–1192.

Channell, J.E.T., 2006. Late Brunhes polarity excursions (Mono Lake, Laschamp, Iceland Basin and Pringle Falls) recorded at ODP Site 919 (Irminger Basin). Earth Planet. Sci. Lett 244, 378–393.

Channell, J.E.T., Hodell, D.A., Curtis, J.H., 2012. ODP Site 1063 (Bermuda Rise) revisited: oxygen isotopes, excursions and paleointensity in the Brunhes Chron. Geochem., Geophys., Geosyst. 13, Q02001, http://dx.doi.org/10.1029/2011GC003897.

Christl, M., Lippolt, J., Steinhilber, F., Bernsdorff, F., Mangini, A., 2010. Reconstruction of global ^{10}Be production over the past 250 ka from highly accumulating Atlantic drift sediments. Quat. Sci. Rev. 29, 2663–2672.

Cox, S.E., Farley, K.A., Memming, S.R., 2012. Insights into the age of the Mono Lake Excursion and magmatic crystal residence time from (UTh)/He and ^{230}Th dating of volcanic allanite. Earth Planet. Sci. Lett 319-320, 178–184.

Dansgaard, W., Johnson, S.J., Clausen, H.B., Dahl-Jensen, D., Gundestrup, N.S., Hammer, C.U., Hvidberg, C.S., Steffensen, J.P., Sveinbjörnsdottir, A.E., Jouzel, J., Bond, G., 1993. Evidence for general instability of past climate from a 250-kyr ice-core record. Nature 364, 218–220.

Denham, C.R., Cox, A., 1971. Evidence that the Laschamp event did not occur 13300-30400 years ago. Earth Planet. Sci. Lett. 13, 181–190.

De Vivo, B., Rolandi, G., Gans, P.B., Calvert, A., Bohrson, W.A., Spera, F.J., Belkin, H.E., 2001. New constraints on the pyroclastic eruptive history of the Campanian volcanic Plain (Italy). Mineral. Petrol 73, 47–65.

Frank, M., Schwarz, B., Baumann, S., Kubik, P.W., Suter, M., Mangini, A., 1997. A 200 kyr record of cosmogenic radionuclide production rate and geomagnetic field intensity from ^{10}Be in globally stacked deep-sea sediments. Earth Planet. Sci. Lett. 149, 121–129.

Fisher, R.A., 1953. Dispersion on a sphere. Proc. R. Soc. Lond. 217A, 295–305.

Fleitmann, D., Cheng, H., Badertscher, S., Edwards, R.L., Mudelsee, M., Göktürk, O.M., Frankhauser, A., Pickering, R., Raible, C.C., Matter, A., Kramers, J., Tüysüz, O., 2009. Timing and climatic impact of Greenland interstadials recorded in stalagmites from northern Turkey. Geophys. Res. Lett. 36, L19707, http://dx.doi.org/10.1029/2009GL040050.

Giaccio, B., Isaia, R., Fedele, F.G., Di Canzo, E., Hoffecker, J., Ronchitelli, A., Sinitsyn, A.A., Anikovich, M., Lisitsyn, S.N., Popov, V.V., 2008. The Campanian Ignimbrite and Codola tephra layers: Two temporal/stratigraphic markers for the Early Upper Palaeolithic in southern Italy and eastern Europe. J. Volc. Geotherm. Res 177, 208–226.

Gillot, P.Y., Labeyrie, J., Laj, C., Valladas, G., Guèrin, G., Poupeau, G., Delibrias, G., 1979. Age of the Laschamp paleomagnetic excursion revisited. Earth Planet. Sci. Lett. 42, 444–450.

Guillou, H., Singer, B.S., Laj, C., Kissel, C., Scaillet, S., Jicha, B.R., 2004. On the age of the Laschamp excursion. Earth Planet. Sci. Lett. 227, 331–343.

Heller, F., Petersen, N., 1982. Self-reversal explanation for the Laschamp/Olby geomagnetic field excursion. Phys. Earth Planet. Inter 30, 358–372.

Jicha, B.R., Kristjánsson, L., Brown, M.C., Singer, B.S., Beard, B.L., Johnson, C.M., 2011. New age for the Skálamælifell excursion and identification of a global geomagnetic event at 94 ka. Earth Planet. Sci. Lett. 310, 509–517.

Kempema, E.W., Reimnitz, E., Barnes, P.W., 2001. Anchor-ice formation and ice rafting in Southwestern Lake Michigan, USA. J. Sediment. Res 71, 346–354.

Kent, D.V., Hemming, S.R., Turrin, B.D., 2002. Laschamp Excursion at Mono Lake? Earth Planet. Sci. Lett 197, 151–164.

Kirschvink, J.L., 1980. The least-squares line and plane and the analysis of palaeomagnetic data. Geophys. J. R. Astr. Soc 62, 699–718.

Kissel, C., Guillou, H., Laj, C., Carracedo, J.C., Nomade, S., Perez-Torrado, F., Wandres, C., 2011. The Mono Lake excursion recorded in phonolitic lavas

from Tenerife (Canary Islands): Paleomagnetic analyses and coupled K/Ar and Ar/Ar dating. Phys, Earth Planet. Inter 187, 232–244.
Korte, M., Constable, C.G., 2005. The geomagnetic dipole moment over the last 7000 years - new results from a global model. Earth Planet. Sci. Lett 236, 348–358.
Krása, D., Shcherbakova, V.P., Kunzmann, T., Petersen, N., 2005. Self-reversal of remanent magnetization in basalts due to partially oxidized titanomagnetites. Geophys. J. Int. 162, 115–136.
Kwiecien, O., Arz, H.W., Lamy, F., Wulf, S., Bahr, A., Röhl, U., Haug, G.H., 2008. Estimated reservoir ages of the Black Sea since the last glacial. Radiocarbon 50, 1–20.
Laj, C., Channell, J.E.T., 2007. Geomagnetic excursions. In: Schubert, G., Bercovici, D., Dziewonski, A., Hering, T., Kanamori, H., Kono, M., Olson, P.L., Price, G.D., Romanowicz, B., Spohn, T., Stevenson, D., Watts, A.B. (Eds.), Treatise on Geophysics, Geomagnetism, vol. 5. Elsevier, B.V, Amsterdam, pp. 373–416.
Laj, C., Kissel, C., Beer, J., 2004. High resolution global paleointensity stack since 75 kyr (GLOPIS-75) calibrated to absolute values. In: Channell, J.E.T., Kent, D.V., Lowrie, W., Meert, J.G. (Eds.), Timescales of the Paleomagnetic Field, Geophys. Monogr, 145. Am. Geophys. Union, Washington, D.C., pp. 255–265.
Laj, C., Kissel, C., Davies, C., Gubbins, D., 2011. Geomagnetic field intensities and inclination records from Hawaii and the Réunion island: geomagnetic implications. Phys. Earth Planet. Inter 187, 170–187.
Laj, C., Kissel, C., Mazaud, A., Channell, J.E.T., Beer, J., 2000. North Atlantic palaeointensity stack since 75 ka (NAPIS75) and the duration of the Laschamp event. Phil Trans. R. Soc. Lond. A 358, 1009–1025.
Laj, C., Kissel, C., Roberts, A.P., 2006. Geomagnetic field behaviour during the Iceland Basin and Laschamp geomagnetic excursions: A simple transitional field geometry? Geochem. Geophys. Geosyst 7, Q03004, http://dx.doi.org/10.1029/2005GC001122.
Levi, S., Audunsson, H., Duncan, R.A., Kristjansson, L., Gillot, P.Y., Jakobsson, S.P., 1990. Late Pleistocene geomagnetic excursion in Icelandic lavas: confirmation of the Laschamp geomagnetic excursion. Earth Planet. Sci. Lett. 96, 443–457.
Liddicoat, J.C., Coe, R.S., 1979. Mono Lake geomagnetic excursion. J. Geophys. Res. 84, 261–271.
Lund, S.P., Liddicoat, J.C., Lajoie, K.R., Henyey, T.L., Robinson, S.W., 1988. Paleomagnetic evidence for long-term (104 year) memory and periodic behavior in the earth's core dynamo process. Geophys. Res. Lett. 15, 1101–1105.
Lund, S.P., Schwartz, M., Keigwin, L., Johnson, T., 2005. Deep-sea sediment records of the Laschamp geomagnetic field excursion (~41,000 calendar years before present). J. Geophys. Res. 110, B04101, http://dx.doi.org/10.1029/2003JB002943.
Lund, S., Stoner, J.S., Channell, J.E.T., Acton, G., 2006. A summary of Brunhes paleomagnetic field variability recorded in Ocean Drilling Program cores. Phys. Earth Planet. Inter 156, 194–204.
Major, C.O., Goldstein, S.L., Ryan, W.B.F., Lericolais, G., Piotrowski, A.M., Hajdas, I., 2006. The co-evolution of Black Sea level and composition through the last deglaciation and its paleoclimatic significance. Quat. Sci. Rev. 25, 2031–2047.
Masarik, J., Beer, J., 1999. Simulation of particle fluxes and cosmogenic nuclide production in the Earth's atmosphere. J. Geophys. Res. 104, 12,099–12,111.
Mochizuki, N., Tsunakawa, H., Shibuya, H., Cassidy, J., Smith, I.E.M., 2006. Palaeointensities of the Auckland geomagnetic excursions by the LTD-DHT Shaw method. Phys. Earth Planet. Inter 154, 168–179.
Muscheler, R., Beer, J., Wagner, G., Laj, C., Kissel, C., Raisbeck, G.M., Yiou, F., Kubik, P.W., 2004. Changes in the carbon cycle during the last deglaciation as indicated by the comparison of ^{10}Be and ^{14}C records. Earth Planet. Sci. Lett. 219, 325–340.
Müller, U.C., Pross, J., Tzedakis, P.C., Gamble, C., Kotthoff, U., Schmiedl, G., Wulf, S., Christianis, K., 2011. The role of climate in the spread of modern humans into Europe. Quat. Sci. Rev. 30, 273–279.
NGRIP (North Greenland Ice Core Project) members, 2004. High resolution record of Northern hemisphere climate extending into the last interglacial period. Nature 431, 147–151.
Nowaczyk, N.R., 1997. High-resolution magnetostratigraphy of four sediment cores from the Greenland Sea II - Rock magnetic and palaeointensity data. Geophys. J. Int 131, 325–334.
Nowaczyk, N.R., Antonow, M., Knies, J., Spielhagen, R.F., 2003. Further rock magnetic and chronostratigraphic results on reversal excursions during the last 50 ka as derived from northern high latitudes and discrepancies in precise AMS^{14}C dating. Geophys. J. Int 155, 1065–1080.
Nowaczyk, N.R., Baumann, M., 1992. Combined high-resolution magnetostratigraphy and nannofossil biostratigraphy for late Quaternary Arctic Ocean Sediments. Deep-Sea Res 39, 567–601.
Plenier, G., Valet, J.-P., Guérin, G., Lefèvre, J.-C., LeGoff, M., Carter-Stiglitz, B., 2007. Origin and age of the directions recorded during the Laschamp event in the Chaîne des Puys. Earth Planet. Sci. Lett. 259, 414–431.
Pyle, D.M., Ricketts, G.D., Margari, V., van Andel, T., Sinitsyn, A.A., Praslov, N.D., Lisitsyn, S., 2006. Wide dispersal and deposition of distal tephra during the Pleistocene 'Campanian Ignimbrite/Y5′ eruption, Italy. Quat. Sci. Rev. 25, 2713–2728.
Raisbeck, G.M., Yiou, F., Bourles, D., Kent, D.V., 1985. Evidence for an increase in cosmogenic ^{10}Be during a geomagnetic reversal. Nature 315, 315–317.
Raisbeck, G.M., Yiou, F., Bourles, D., Lorius, C., Jouzel, J., Barkov, N.I., 1987. Evidence for two intervals of enhanced ^{10}Be deposition in Antarctic ice during the last glacial period. Nature 326, 273–277.
Reimer, P.J., Baillie, M.G.L., Bard, E., Bayliss, A., Beck, J.W., Blackwell, P.G., Ramsey, C.B., Buck, C.E., Burr, G.S., Edwards, R.L., Friedrich, M., Grootes, P.M., Guilderson, T.P., Hajdas, I., Heaton, T.J., Hogg, A.G., Hughen, K.A., Kaiser, K.F., Kromer, B., McCormac, F.G., Manning, S.W., Reimer, R.W., Richards, D.A., Southon, J.R., Talamo, S., Turney, C.S.M., van der Plicht, J., Weyhenmeyer, C.E., 2009. IntCal09 and Marine09 radiocarbon age calibration curves, 0–50,000 years cal BP. Radiocarbon 51, 1111–1150.
Reynolds, R.L., Tuttle, M.L., Rice, C.A., Fishman, N.S., Karachewski, J.A., Sherman, D.M., 1994. Magnetization and geochemistry of greigite-bearing Cretaceous strata, North Slope basin, Alaska. Am. J. Sci 294, 485–528, http://dx.doi.org/10.2475/ajs.294.4.485.
Roberts, A.P., 1995. Magnetic properties of sedimentary greigite (Fe_3S_4). Earth Planet. Sci. Lett. 134, 227–236.
Roberts, A.P., 2008. Geomagnetic excursions: knowns and unknowns. Geophys. Res. Lett. 35, L17307, http://dx.doi.org/10.1029/2008GL034719.
Roberts, A.P., Turner, G.M., 1993. Diagenetic formation of ferrimagnetic iron sulphide minerals in rapidly deposited marine sediments, South Island, New Zealand. Earth Planet. Sci. Lett. 115, 257–273.
Roberts, A.P., Winklhofer, M., 2004. Why are geomagnetic excursions not always recorded in sediments? Constraints from post-depositional remanent magnetization lock-in modelling. Earth Planet. Sci. Lett 227, 345–359.
Ron, H., Nowaczyk, N.R., Frank, U., Schwab, M.J., Naumann, R., Striewski, B., Agnon, A., 2007. Greigite detected as dominating remanence carrier in Late Pleistocene sediments, Lisan Formation, from Lake Kinneret (Sea of Gallilee, Israel). Geophys. J. Int. 170, 117–131.
Roperch, P., Bonhommet, N., Levi, S., 1988. Paleointensity of the earth's magnetic field during the Laschamp excursion and its geomagnetic implications. Earth Planet. Sci. Lett 88, 209–219.
Ross, D.A., Degens, E.T., 1974. Recent sediments of Black Sea. In: Degens, E.T., Ross, D.A. (Eds.), The Black Sea – geology, chemistry, and biology. Am. Assoc. Petroleum Geologists Mem, 20; 1974, pp. 183–199.
Rowan, C.J., Roberts, A.P., Broadbent, T., 2009. Reductive diagenesis, magnetite dissolution, greigite growth and paleomagnetic smoothing in marine sediments: A new view. Earth Planet. Sci. Lett. 277, 223–235.
Röhl, U., Abrams, L.J., 2000. High resolution, downhole, and non-destructive core measurements from sites 999 and 1001 in the Caribbean Sea: application to the late Paleocene thermal maximum. Proc. Ocean Drill. Prog. Sci. Res 165, 191–204.
Singer, B., Guillou, H., Jicha, B.R., Laj, C., Kissel, C., Beard, B.L., Johnson, C.M., 2009. ^{40}Ar/^{39}Ar, K-Ar and ^{230}Th-^{238}U dating of the Laschamp excursion: A radioisotopic tie-point for ice core and climate chronologies. Earth Planet. Sci. Lett. 286, 80–88.
Snowball, I., 1991. Magnetic hysteresis properties of greigite (Fe_3S_4) and a new occurrence in Holocene sediments from Swedish Lappland. J. Quat. Sci 68, 32–40.
Snowball, I., Thompson, R., 1990. A stable chemical remanence in Holocene sediments. J. Geophys. Res. 95, 4471–4479.
Svensson, A., Andersen, K.K., Birgler, M., Clausen, H.B., Dahl-Jensen, D., Davies, S.M., Johnsen, S.J., Muscheler, R., Rasmussen, S.O., Röthlisberger, R., Steffensen, J.P., Vinther, B.M., 2006. The greenland ice core project 2005, 15-42 ka. Part 2: comparison to other records. Quat. Sci. Rev. 25, 3258–3267.
Svensson, A., Andersen, K.K., Birgler, M., Clausen, H.B., Dahl-Jensen, D., Davies, S.M., Johnsen, S.J., Muscheler, R., Parrenin, F., Rasmussen, S.O., Röthlisberger, R., Seierstad, I., Steffensen, J.P., Vinther, B.M., 2008. 60 000 year Greenland stratigraphic ice core chronology. Clim. Past 4, 47–57.
Teanby, N., Laj, C., Gubbins, D., Pringle, M., 2002. A detailed palaeointensity and inclination record from drill core SOH1 on Hawaii. Phys. Earth Planet. Inter 131, 101–140.
Valet, J.-P., Plenier, G., 2008. Simulations of a time-varying non-dipole field during geomagnetic reversals and excursions. Phys. Earth Planet. Inter 169, 178–193.
Valet, J.-P., Plenier, G., Herrero-Bervera, E., 2008. Geomagnetic excursions reflect an aborted polarity state. Earth Planet. Sci. Lett. 274, 472–478.
Wagner, B., Zanchetta, G., Wessels, M., Nowaczyk, N., 2008. The last 40 ka tephrostratigraphic record of Lake Ohrid, Albania and Macedonia: a very distal archive for ash dispersal from Italian volcanoes. J. Volc. Geotherm. Res 177, 71–80.
Winguth, C., Wong, H.K., Panin., N., Dinu, C., Georgescu, P., Ungureano, G., Krugliakov, V.V., Podshuveit, V., 2000. Upper Quaternary water level history and sedimentation in the northwestern Black Sea. Mar. Geol 167, 127–146.
Wulf, S., Kraml, M., Brauer, A., Keller, J., Negendank, J.F.W., 2004. Tephrochronology of the 100 ka lacustrine sediment record of Lago Grande di Monticchio (southern Italy). Quat. Int 122, 7–30.
Zimmerman, S.H., Hemming, S.R., Kent, D.V., Searle, S.Y., 2006. Revised chronology for late Pleistocene Mono Lake sediments based on paleointensity correlation to the global reference curve. Earth Planet. Sci. Lett. 252, 94–106.